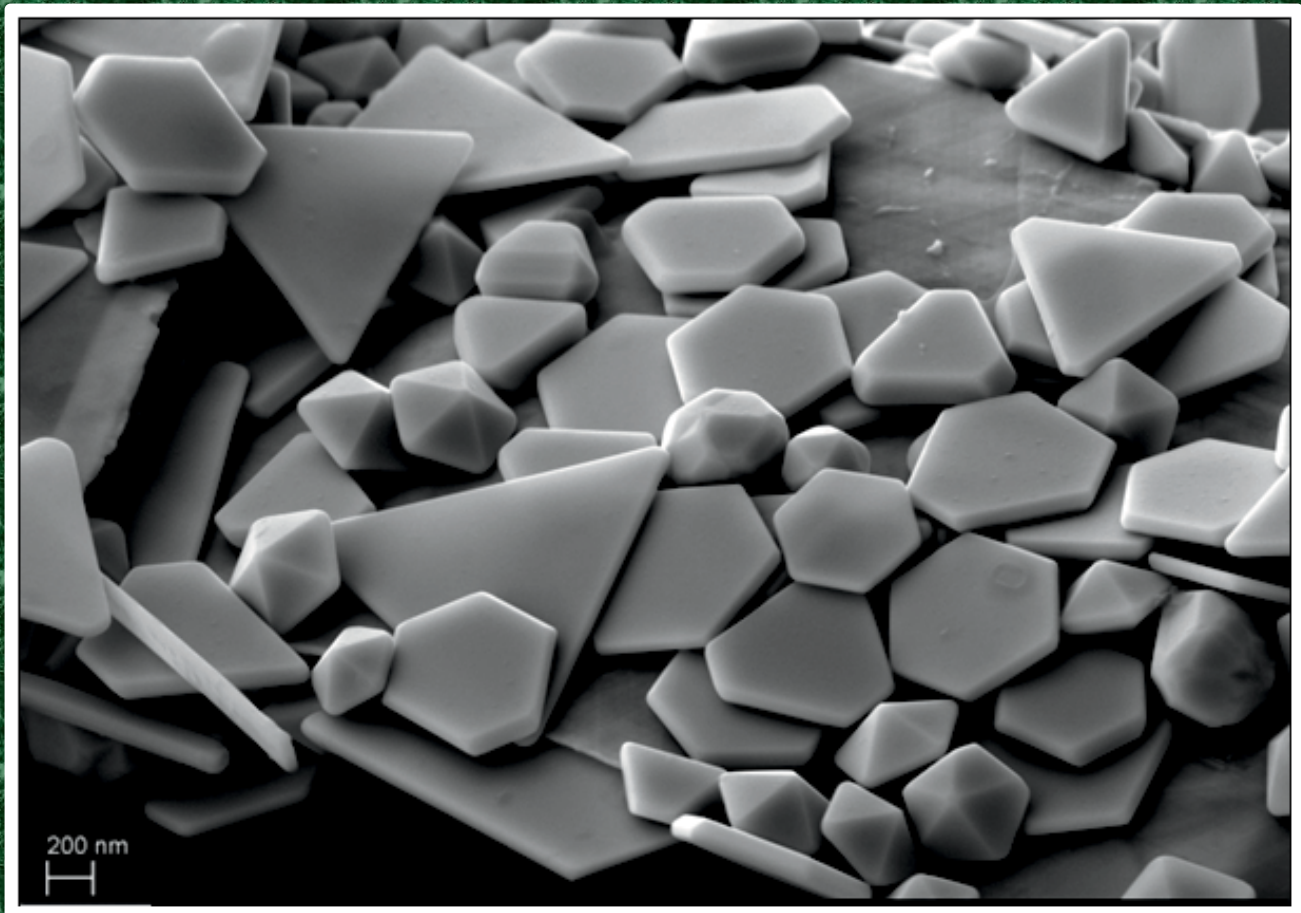


Texas Journal of Microscopy



Volume 54
Number 1, 2023
ISSN 1554-0820

Visit our website at www.texasmicroscopy.org

Providing Microscopy Supplies and Specimen Preparation Equipment to Our Valued Customers for Over Half a Century



PELCO® Scribing & Cleaving Solutions

PELCO® LatticeAx® 420, PELCO® FlipScribe® & PELCO® FlexScribe™



Cressington Coating Systems

Carbon Evaporation & Metal Sputtering Accessories & Targets



PELCO BioWave® Pro+

Microwave Tissue Processor & Application Kits



Now Available from Ted Pella, Inc.

DIATOME®

Highest Quality Diamond Knives Available for All Applications



PELCO easiGlow™

Cryo-EM Glow Discharge Set including Vacuum Pump with Accessories, Gasket & PELCO® Grid Holder Block



Cryo-EM Tools & Accessories

Large Dewars, Foam Dewars, Grid Boxes & Grippers, Tweezers, Cryo-Pins & Storage



NEW First Contact™ Photonic Cleaning Solution Kit



NEW Sizes Available PELCO Tabs™ Carbon Tabs



NEW PELCO® Qualitative Cellulose Filter Paper



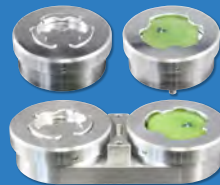
NEW Kulzer Technovit® Acrylic Resin Systems



PELCO® Modular SEM Mounts & Holders



NEW Brass & Copper SEM Mounts



NEW Top Referencing Metallographic Mount Holders



NEW t-EBSD Holders & FIB Lift-Out Grids

TED PELLA, INC.
Microscopy Products for Science and Industry

www.tedpella.com sales@tedpella.com 800-237-3526

TSM OFFICERS 2022-2023

President:

AMY JO HAMMETT
Division of Biology, School of the Sciences
Texas Woman's University, Denton, TX 76204-5799
(940) 898-2397; Ahammett1@twu.edu

President-elect:

JOSEFINA ARELLANO
MSE Core Characterization Facility
The University of Texas at Dallas, Richardson, TX, 75080
(972) 883-5759; Josefina.Arellano@utdallas.edu

Past President:

BERND ZECHMANN
Center for Microscopy and Imaging
Baylor University, Waco, TX 76798-7046
(254) 710-2322; Bernd_Zechmann@baylor.edu

Secretary:

BERND ZECHMANN
Center for Microscopy and Imaging
Baylor University, Waco, TX 76798-7046
(254) 710-2322; Bernd_Zechmann@baylor.edu

Secretary-elect:

AMY JO HAMMETT
Division of Biology, School of the Sciences
Texas Woman's University, Denton, TX 76204-5799
(940) 898-2397; Ahammett1@twu.edu

Treasurer:

DAVID GARRETT
Dept. of Materials Science and Engineering
University of North Texas, Denton, Texas 76203-5017
(940) 369-8836; dgarrett@unt.edu

Treasurer-elect:

BERND ZECHMANN
Center for Microscopy and Imaging
Baylor University, Waco, TX 76798-7046
(254) 710-2322; Bernd_Zechmann@baylor.edu

Program Chairperson:

JOSEFINA ARELLANO
MSE Core Characterization Facility
The University of Texas at Dallas, Dallas, Richardson, TX
75080
(210) 458-8735; josefina.arellano@utdallas.edu

Program Chairperson-elect:

VACANT

APPOINTED OFFICERS

Corporate Member Representative:

JAMES C. LONG
Ted Pella, Inc.
P.O. Box 492477, Redding, CA 96049
(530) 227-8329; james_long@tedpella.com

Facebook Master:

NABARUN GHOSH
Department of Life, Earth, and Environmental Sciences
West Texas A&M University, Canyon, Texas 79015
(806) 651-2571; FAX (806) 651-2928; nghosh@wtamu.edu

Student Representative:

LYANNA DELEON
Department of Life, Earth, and Environmental Sciences
West Texas A&M University, Canyon, Texas 79015
(806) 341-4771; ldeleon1@buffs.wtamu.edu

Journal Editors:

CATALINA PISLARIU
Division of Biology, School of the Sciences
Texas Woman's University, Denton, TX 76204-5799
(940) 898-4611; cpislariu@twu.edu

Webmaster:

BERND ZECHMANN
Center for Microscopy and Imaging
Baylor University, Waco, TX 76798-7046
(254) 710-2322; Bernd_Zechmann@baylor.edu

Contents

TEXAS JOURNAL OF MICROSCOPY
VOLUME 54, NUMBER 1, 2023
ISSN 1554-0820



Editor

Catalina Iulia Pislariu, PhD
Division of Biology, School of the Sciences,
Texas Woman's University, Denton, TX 76204

Official Journal of the Texas Society for Microscopy

"TSM - Embracing all forms of Microscopy"

www.texasmicroscopy.org

President's Message	5
Keynote Speakers for the 57th TSM Meeting	6
Spring 2023 Life Sciences Abstracts	9
Spring 2023 Material Sciences Abstracts	17
Spring 2023 Technical Abstracts	24
Corporate Members	31
Advertiser's Index:	
Ted-Pella	2
DIATOME	4
Electron Microscopy Sciences	35
Tousimis	36

ON THE COVER

The cover image shows a variety of structures made of gold. Most nanoparticles look flat and of uniform thickness. The smaller ones comprise of a range of shapes, including polyhedra with five-fold symmetry. The image was acquired by Scanning Electron Microscopy; signal: secondary electrons; operating voltage: 10 keV. Courtesy of Dr. Maria Josefina Arellano—Jimenez, Department of Material Science and Engineering, University of Texas at Dallas.

DiATOME Diamond Knives

the incomparable
Diamond Knife for
all fields of research...

Please visit our website
for our complete range
of Diamond Knives:
www.diatomeknives.com

ultra Maxi

Similar to our ultra 35° 4.0 mm but with a larger boat. Applications include soft industrial samples such as metals and polymers, hard and brittle samples such as semiconductors, superconducting oxides, nanocrystalline ceramics.

Rat muscle (Quadriceps) x
23'000 Werner Graber,
Anatomisches Institut, Bern



Eye of *A. peroni*: part of a sequence of semithin sections. Michael J.F. Blumer, Institut für Zoologie, Universität Wien. Reprinted from: Ribbons of semithin sections an advanced method with a new type of diamond knife. *Journal of Neuroscience Methods* 120 (2002 11-16), with permission from Elsevier. See the complete series on diatomeknives.com.

histo Jumbo

Perfect for Immuno-histo-chemistry

For 3D reconstruction it is imperative not to lose a single section (Ref. Blumer). The large Jumbo boat as well as the adhesive (Pattex compact by Henkel) applied to the side of the sample block increase the distinct advantages. They allow:

- Easy production of section ribbons (0.5-2 µm)
- No section loss
- No folding
- The same orientation of all sections
- Easy collection of section ribbons
- Multiple ribbons on one glass slide

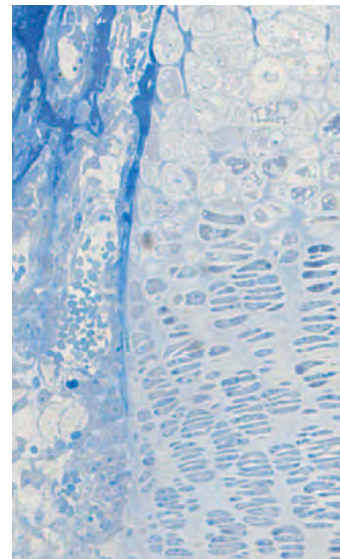
histo

The knife is designed for the sectioning of hard and soft biological and industrial materials, non embedded or embedded in methacrylate or epoxy resins. The histo knife may be used on all ultramicrotomes and microtomes with a retraction of the specimen in the return phase.

Advantages compared to glass knives:

- Perfect sections, free of scores or compression.
- Serial sections without knife change.
- Thinner sections.

Nondecalcified rat bone.,
Scale: 35 mm = 100µm.
Daniel Studer, Anatomisches
Institut, Bern.



DiATOME U.S.

P.O. Box 410 • 1560 Industry Rd. • Hatfield, Pa 19440
Tel: (215) 412-8390 • Fax: (215) 412-8450
email: info@diatomeknives.com

President's Message

This year we come together again to celebrate our shared love of microscopy and foster fellowship amongst our members at the 57th annual TSM meeting at UT Dallas in Richardson. On behalf of the Texas Society for Microscopy (TSM), I would like to thank our program chairperson Josefina Arellano Jimenez for organizing this year's annual TSM meeting. I am grateful to our corporate sponsors Thermo Fisher and Protochips for their sponsorship of the outstanding workshops at the Natural Science and Engineering Research Laboratory at UT Dallas. We are very proud to support and display the hard work of our members in the form of platform and poster presentations. I want to personally thank this year's invited speakers for their support of the TSM, Daniela Nicastro from UT Southwestern Medical Center, Alice Liang from New York University Grossman School of Medicine, and Moon Kim from UT Dallas.

I would like to express much gratitude the Executive Board of the TSM for their service and dedication to the organization. I would like to thank our journal editor, Catalina Pislariu, for doing an amazing job editing and publishing the Texas Journal of Microscopy. Thanks to our treasurer, David Garrett, the financial situation of our society is in a very good state. I am always amazed by and very grateful for the support of our secretary Bernd Zechmann for managing the business and communications of the TSM. I am also thankful for the tireless support of James Long and Lyanna DeLeon,

who do an amazing job representing and increasing the participation of the corporate sponsors and student members of the TSM. Finally, I am grateful to Nabarun Ghosh for his support as the social media representative.

Many thanks also go out to all our regular members, student members, honorary members, and corporate members for your support of the TSM with your membership and your participation at our annual meeting. It has been an honor and pleasure to serve as President of the TSM for the last two years. I am looking forward to supporting the next president Josefina Arellano-Jimenez and wish her and the TSM the most success.

Amy Jo Hammett
TSM President, 2022-2023



INVITED SPEAKER

PROBING THE MOLECULAR ORGANIZATION AND FUNCTION OF CELLS USING CRYO-ELECTRON TOMOGRAPHY

DANIELA NICASTRO

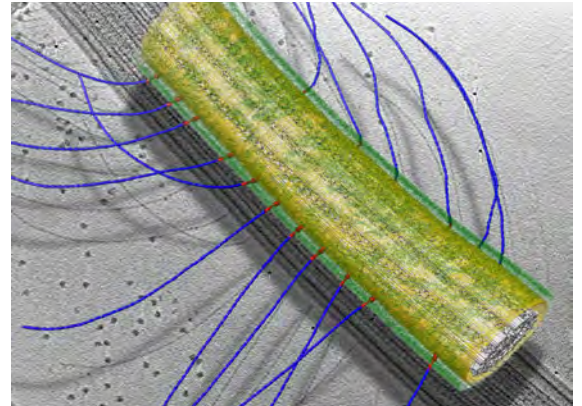
Professor

Department of Cell Biology, UT Southwestern Medical Center, Dallas, TX

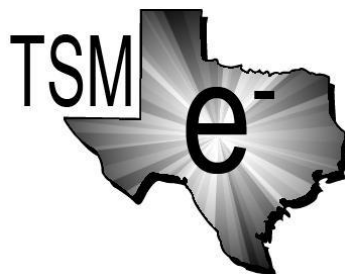


Rapid freezing of cells can provide outstanding structure preservation and time resolution of dynamic cellular processes. Electron tomography of rapidly frozen specimens (cryo-ET) is a powerful technique for imaging biological structures in their native state and in an unperturbed cellular environment. Integrating cryo-ET and sub-tomogram averaging with comparative genetics, biochemical methods and EM-visible labeling allows visualization of the *in-situ* 3D structure and functional organization of macromolecular complexes and organelles inside cells. One of the model systems that we study are cilia, which are conserved and ubiquitous eukaryotic organelles. Motile cilia are composed of more than 600 different proteins, have important biological roles in motility and sensation, and defects in their assembly or function cause severe human diseases. Our cryo-ET studies have visualized the 3D structures of wild-type and mutant cilia, dissected the organization of key macromolecular complexes in different functional states, and revealed the molecular mechanisms of

how cilia beat. We are also advancing and applying cryo-focused ion beam milling to generate sections (“lamella”) from biological samples that would otherwise be too thick (> a few hundred nanometers) for cryo-ET. Using latter approach, we study cytoskeletal assemblies and cellular machines inside model organisms ranging from yeast to worms. Our findings provide detailed insights into the structural basis and ultimately the function of many cellular processes.



Dr. Daniela Nicastro joined the UT Southwestern Medical Center in 2015, where she established a new state-of-the art cryo-electron microscopy core facility in parallel to running her own research lab. She is a Cancer Prevention and Research Institute of Texas Scholar, was named a Pew Biomedical Scholar, a Keith R. Porter Fellow, and received the 2020 WICB (Women in Cell Biology) Mid-Career Award for Excellence in Research from the American Society for Cell Biology. Dr. Daniela Nicastro has more than 30 years of experience in electron microscopy of cellular structures and continues to make both technical and biological contributions to the field of structural cell biology.



TEXAS SOCIETY FOR MICROSCOPY 57TH ANNUAL MEETING

KEYNOTE SPEAKER PRESENTATIONS

A RESEARCH DRIVEN MICROSCOPY CORE OPERATION AND OPTIMAL DIVERSE BIOLOGICAL SAMPLE PREPARATION METHODS FOR 2D AND 3D ELECTRON MICROSCOPY IMAGING

ALICE (FENG-XIA) LIANG

Research Professor and Director of the Microscopy Core Laboratory

Division of Advanced Research Technologies, New York University Grossman School of Medicine, New York, USA



With the rapid development of various microscopy technologies and methods, centralized research resource facilities that provide access to advanced instrumentation, and professional expertise are important to the research community. Established in 2005 and sited in a fast-growing medical school, the Microscopy Core Laboratory of NYU Grossman School of Medicine expanded from an electron microscopy core to a school-wide imaging core to cover both light and electron microscopy services for more than 190 NYU laboratories and 50 external academic institutions and industries. This presentation will give an overview of the microscopy core operations and focus on technical strategies of optimal preservation of ultrastructure for biological samples ranging from *in vitro* cultured cells to parasites and mammalian tissues, from high resolution two-dimensional and three-dimensional imaging to image presentation.

Dr. Alice (Feng-Xia) Liang is the Director of the Microscopy Laboratory and Research Professor of Cell Biology at the New York University Grossman School of Medicine. She is currently serving as a MSA council and Biology Director. She designs protocols for all electron microscopy projects, has expertise for immune-electron microscopy in 2D and 3D.



TEXAS SOCIETY FOR MICROSCOPY 57TH ANNUAL MEETING

KEYNOTE SPEAKER PRESENTATIONS

DISCOVERY OF NEW NANOMATERIAL PHASES AND NanoArt

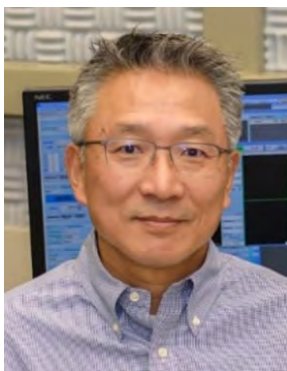
MOON J. KIM

Professor

Department of Materials Science and Engineering

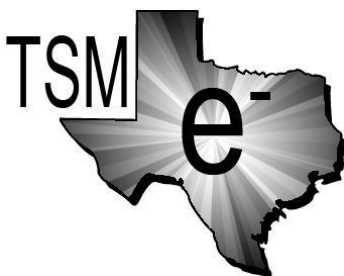
The University of Texas at Dallas, Richardson, TX

<http://moonkim.org/>; moonkim@utdallas.edu



With the advancement of new technology/computation in the era of materials genome, we are studying the ever-increasing number of new and emerging materials for potential new applications. Moreover, we often deal with non-conventional processes or non-equilibrium conditions for the fabrication and processing of materials. That provides ample opportunities for finding new material phases not predicted by phase diagrams or theory. In particular, atomic-resolution electron microscopy combined with various *in-situ* capabilities offers fertile ground for discovering new materials/phases. I present two new material phases recently discovered: • Mo₆Te₆ nanowire and • various forms of tellurium, such as helical Te and 2D Tellurene. In addition, I will introduce “NanoArt,” a new discipline that discovers and accentuates the artistic beauty of nanometer-sized natural and artificial materials, and will showcase some of my NanoArt collections and Artificial Intelligent (AI) stylized NanoArt pieces.

Moon Kim is a Louis Beecherl, Jr., Distinguished Materials Science and Engineering Professor at the University of Texas at Dallas. He is an elected fellow of the Microscopy Society of America and a co-founder of 2Lux Media, Inc. He has published over 460 refereed journal articles, 2 paper books, 2 iBooks, and 1 app-book. He has also held 2 NanoArt exhibitions. Dr. Kim’s current research includes nanoscale fabrication and atomic-scale characterization of various functional nanostructures/devices for applications in nano-electronics, power electronics, energy, electrochemical and bio-devices, 3D visualization technologies such as Virtual Reality (VR), Augmented Reality (AR), image recognition, and hologram for enhanced education, and artificial intelligence (AI) platforms for emerging applications.



Abstracts

LIFE SCIENCES Spring 2023

SYNTHESIS OF TeO_2 NANOPARTICLES FOR BIOMEDICAL APPLICATIONS. T. HESABIZADEH^{1,2}, G. GUISBIERS²

¹ Department of Biology, University of Arkansas at Little Rock, Little Rock, AR 72204

² Department of Physics and Astronomy, University of Arkansas at Little Rock, Little Rock, AR 72204
tthesabizade@ualr.edu; gguisbiers@ualr.edu

Tellurium dioxide (TeO_2) has been synthesized by pulsed laser ablation in liquids. The nanoparticles were spherical with a size distribution centered around ~ 70 nm. The main advantage of this synthesis methodology is that it gives nanoparticles a clean surface, allowing them to interact with bacteria more effectively. One Gram-positive and one Gram-negative bacterial strains were examined in this experiment (Multidrug-resistant *Escherichia coli* and Methicillin-resistant *Staphylococcus aureus*). At concentrations of less than approximately 10 parts per million (ppm), TeO_2 nanoparticles were effective in annihilating both types of bacteria. TeO_2 nanoparticles were also successfully tested against melanoma.

References:

Tina Hesabizadeh, Evan Hicks, David Medina Cruz, Shawn E Bourdo, Fumiya Watanabe, Marvin Bonney, John Nichols, Thomas J Webster, Grégory Guisbiers, *Synthesis of "Naked" TeO_2 Nanoparticles for Biomedical Applications*, *ACS Omega* (2022) vol. 7, 23685-23694, <https://doi.org/10.1021/acsomega.2c02316>

NETWORK OF ROD/CONE GAP JUNCTIONS THROUGH QUANTITATIVE LIGHT/ELECTRON MICROSCOPY. MUNENORI ISHIBASHI^{1,2}, CHRISTOPHE P. RIBELAYGA¹ and STEPHEN C. MASSEY²

¹Department of Vision Sciences, University of Houston College of Optometry, Houston, TX

²Richard Ruiz Department of Ophthalmology and Visual Science, McGovern Medical School, The University of Texas Health Science Center, Houston, TX

Gap junctions (GJs) are intercellular pores that mediate

metabolic and electrical coupling between cells. Composed of connexins, GJs are present in nearly all tissues. Connexin 36 (Cx36) is one of the main connexins to build neural networks in mammalian brain; however, they are small, difficult to image and often ignored in large-scale anatomical analyses of neural circuits. Here we visualize and analyze small Cx36 GJs at photoreceptor terminals in the mouse retina by light and electron microscopy (EM). There are two types of mouse photoreceptors, cone and rod cells. They are electrically coupled via Cx36, providing secondary rod pathway. Light microscopy (LM) revealed the number of Cx36 clusters on a rod or cone, and EM clarified divergence and convergence. Each cone had ~ 50 GJs, while coupled with ~ 40 rods (convergence of 40). Each rod had 2 - 3 GJs, with 2 cones (divergence of 2). From these numbers, we can calculate number of GJs for a pair of rod/cone coupling, 1 - 1.5 GJ. Thus, 40 rods on a cone can make 40 - 60 GJs, consistent with the 50 GJs detected on single cone. Next, we estimated the number of channels from LM and EM. Fluorescence intensity of Cx36 cluster in LM suggested rod/cone GJ is 8 times smaller than that in the inner plexiform layer sublamina b, giving ~ 40 channels. Rod/cone GJ in EM showed electron-dense rectangular structures with length of ~ 500 nm, giving 50 channels. These 40 - 50 channels in a cluster indicates rod/cone GJs are single-string type; channels aligned in a line as imaged by freeze-fracture EM previously (Raviola and Gilula, 1973). The single rod/cone coupling with 1 - 1.5 GJ, or 40 - 80 channels can provide maximum conductance of 1200 pS (15 pS as Cx36 unitary conductance). Rod/cone coupling in mouse shows ~ 1300 pS under Cx36 activation as we reported previously. Thus, we propose that open probability of GJ channels can approach 100% (Ishibashi, et al., 2022).

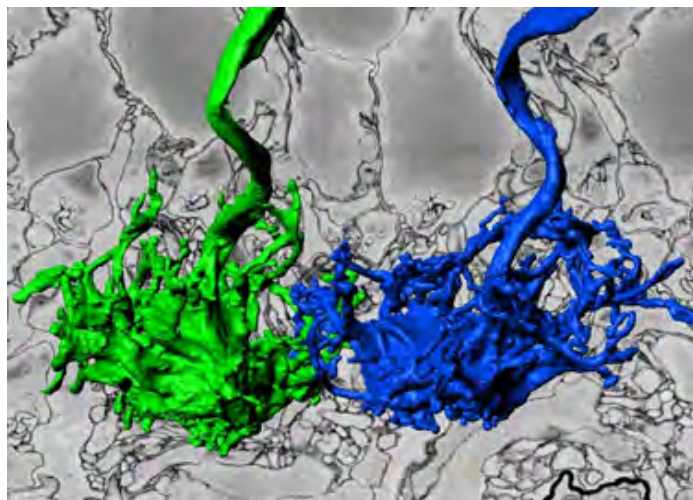


Figure 1: 3D reconstruction of cone pedicles (green and blue) from electron microscopy data (back).

References:

Raviola E and Gilula NB (1973) Gap junctions between photoreceptor cells in the vertebrate retina. *PNAS* 70:1677–1681.

Ishibashi M et al. (2022) Analysis of rod/cone gap junctions from the reconstruction of mouse photoreceptor terminals. *eLife* 11:e73039.

MICROSCOPIC EXAMINATION ON ENVIRONMENTAL POLLUTANTS IN THE AIR CAUSING ADVERSE HEALTH EFFECTS. LYANNA DELEON, MARYTRINH NGUYEN, and NABARUN GHOSH

Department of Life, Earth and Environmental Sciences, West Texas A&M University, Canyon, Texas 79015

Aerosols can be solid or liquid, comprise of organic and/or inorganic material or contain living organisms. Inevitably, some aerosol particles are potentially toxic, allergenic, or infective to people. Various studies reported a correlation between the presence of ammonia (NH³) as the precursor with the biggest impact on the formation of particulate matter (PM_{2.5}) in the air and the incidence of allergy and asthma cases. In recent years, PM_{2.5} has been linked to 4.58 million deaths globally and has been identified as the fifth greatest risk factor for health. Ammonia emissions from agriculture are responsible for 30% of all PM_{2.5} in the US; 44% of the total emissions are being produced globally by cattle. When ammonia is released from agricultural sources, it can then travel in a gaseous state through the atmosphere for short or long distances. Irritation from PM_{2.5} can begin at concentrations as low as 5ppm but are more noticeable at 30ppm. Acute or accidental exposures to high concentrations at 50ppm can result in tracheal burns and damage to bronchial tissues. Therefore, we have been focusing our research to determine the counts of airborne particulate matter including fungal spores in the Texas Panhandle area. We have been utilizing a Burkard Volumetric Spore Trap placed on the rooftop of the Natural Science building of the West Texas A&M University campus. We collected the exposed tape from the spore trap regularly and mounted them on glass slides after dividing them into seven equidistant strips using a standard scale. The tape was stained with 2% Safranin-Gelvatol solution. The solution functions in a dual mode: to stain the trapped materials and as a sealing mountant. We used a BX-40 Olympus Microscope and a DP-74 digital camera. The *CellSense* software was used to acquire images and to analyze the trapped samples collected from the air. There is a significant increase in the concentration of PM_{2.5} in the ambient air, both from organic and inorganic sources, as our data reflected from the spore trap collection in the recent years. The most frequent fungal spores that showed an increase in count were *Alternaria*, *Cladosporium*, *Curvularia*, *Pithomyces* and *Ustilago*. As we analyzed and compared the data from the slides prepared in the last 20 years a significant increase in the number of particulates

was noticed, as we continue to experience climate changes. Recent significant incidence in wildfire cases is highly correlated with the higher rate of the particulate pollution.

FIBRONECTIN-DERIVED FLUORESCENT CARBON DOTS FOR BIOIMAGING APPLICATIONS. SARA STRICKLAND, MYCHELE JORNS, LINDSEY HEYD, and DIMITRI PAPPAS

Department of Chemistry and Biochemistry, Texas Tech University, Lubbock, TX, 79409

Fibronectin (FN) is a glycoprotein well known for its involvement in cellular adhesion, cell mobility and cell growth, due to integrin-mediated signaling. Due to these properties, FN has been known to be upregulated in the extra cellular matrix (ECM) of certain cancer cell lines. For these reasons, FN was selected as the precursor for carbon dot synthesis, and the subsequent targeting of FN found in cancerous cells ECM's. Some carbon dots fluoresce and possess selectivity for specific molecules via tuning synthesis processes. These FN-derived carbon dots exhibit violet fluorescence under ultraviolet excitation, while simultaneously appearing to display selectivity for the FN they are derived from. This is hypothesized to be the result of passivation of the carbon dot surface during the microwave heating process via nitrogen-containing surface functional groups. Cancer cell lines MCF-7 and MDA-231 were stained with these carbon dots, and our observations established that the carbon dots did not pass through the membrane and aggregate within the cell, as seen with other types of carbon dots. Instead, the FN-derived nanoparticles appeared to interact with the outer cell membrane and ECM, where FN is found in abundance. We hypothesize that the FN-derived carbon nanoparticles selectively bind by amide linkages to the FN receptors that are plentiful on the surface of the cell. This hypothesis is supported with EDS and FTIR data confirming the presence of nitrogen containing functional groups like -NH₃ and other surface groups like -COOH. These nanoparticles have bioimaging applications due to their specificity for FN in a cancer cell membrane and their ability to fluoresce under UV light, without the need for post synthesis modifications.

FLUORESCENCE MICROSCOPY AND ASSESSMENT OF GENOTOXICITY OF ATRAZINE ON *DAPHNIA* AND *ALLIUM* TEST SYSTEMS. MARIA LOUISA ZAVALA, and NABARUN GHOSH

Department of Life, Earth & Environmental Sciences, West Texas A&M University, Canyon, Texas 79015.

Fluorescence microscopy is often used to image properties of organic and inorganic substances. It uses optical sectioning to obtain a better resolution of the fluorescence image. While fluorescence is preferred to regular parfocal microscopy, Z-stacking software can also be used in conjunction with fluorescence. This software captures the image by focusing on different parts of the

specimen and then stacking them into one focused image. Fluorescent microscopy allowed us to assess intoxication in *Daphnia magna*. *D. magna* acts as an excellent model organism due to its short life span and high reproductive capability. The *Daphnia* test system is suitable for examining hypotheses and allows for creating simple experimentation tests. Therefore, we have chosen to use *Daphnia* in our study to determine toxicity to the *Daphnids* using the herbicide Atrazine as a subject for our microscopic studies involving lethality caused by chemical pollution. *Allium cepa* is an efficient test system due to its effectiveness in *in-situ* monitoring for the genotoxicity of various environmental contaminants. The testing reveals which of these compounds can induce chromosomal abnormalities in the root meristem of the *A. cepa*. This research aims to examine the genotoxic and lethal effect of Atrazine on the *Daphnia magna* and the *Allium cepa* test systems. Atrazine is a chlorinated triazine systemic herbicide. It is used to control annual grasses and the broadleaf weeds selectively in various crops grown in Texas and the greater United States. While the Environmental Protection Agency (EPA) currently has Atrazine classified as a restricted-use pesticide in the US, the EU has had Atrazine banned since 2006. This was due to the pervasive and unpreventable water contamination that the herbicide caused. Studies have shown that Atrazine is linked to the decline of amphibians and other species. Atrazine is a known endocrine disruptor that affects sexual development in amphibians by changing the hormone cycle. In this study, we aimed to determine the effect of Atrazine on our community health. *Daphnia* have a high sensitivity to environmental pollutants because they are sensitive to toxicants and indicate water pollution. *Daphnids* demonstrate reproductive decline, aberrant vertical mobility, and phenotypic plasticity to name a few when exposed to environmental stressors. Abiotic and biotic stressors include chemical substances, synthetic hormones, acidity, salinity, etc. We tested the survival rate of *Daphnia* at different concentrations of the herbicide and recorded the concentration for the LD50 (Lethal Dose 50). To observe and assess any genotoxic effect of Atrazine, we prepared slides of mitotic plates from root tip squash of *A. cepa* after pre-treatment, fixation and staining with 2% Aceto-Orcein. We excised the root tips from the control set of bulbs and pre-treated them with a saturated solution of para-Dichlorobenzene (p-DB) for 3 hours. After pre-treatment, the root tips were washed with distilled water three times and fixed with 1:3 Aceto-ethanol overnight. The fixed root tips were stained with 2% Aceto-Orcein solution and squashed in 45% acetic acid. Once the slide was prepared, we observed the different phases of cell division and captured the micrographs at various magnifications. We captured the micrographs at various magnifications using a BX-40 Olympus microscope equipped with a DP-74 digital camera and the *CellSens* software. We captured micrographs of *Daphnia* using single focal plane and Z-stacking imaging. We found that *Daphnia* exhibited lethality even with a very low dose of the herbicide (0.01%)

proving that the herbicide is both genotoxic and lethal to the *Daphnids* and *A. cepa* test systems.

References:

- Environmental Protection Agency. (n.d.). EPA. Retrieved February 7, 2023, from <https://www.epa.gov/ingredients-used-pesticide-products/atrazine>
- Le, V. Q., Choi, W., Kim, T., Woo, S. M., Kim, Y.-H., & Min, J. (2020). *In vivo* assessment of pathogens toxicity on *Daphnia magna* using fluorescent dye staining. *Ecotoxicology*, 29(7), 892–899. <https://doi.org/10.1007/s10646-020-02257-6>
- Ghosh N. and M. Whiteside. (2006d). Fluorescent Microscopy in characterizing some biological specimens. *Journal of Scanning Microscopies*, Vol. 28, No. 2 (March/ April 2006):129-130.
- Ghosh N., Finger, K., Usnick, S., Rogers, W.J., Das, A. B. and Smith, D.W. (2010). Microscopic examination on cytological changes in *Allium cepa* and shift in phytoplankton population at different doses of Atrazine. *Scanning Microscopy 2010* (edited by Michael T. Postek, Dale E. Newbury, S. Frank Platek, David C. Joy.); SPIE Vol. 7729 Sec. W-1:1-14.

SEM IMAGING OF NATIVE PLANT SEEDS FOR BUILDING A SEED DATABASE. ANJOLA IFAGBAYI-ADENIRAN and CAMELIA MAIER

Division of Biology, School of the Sciences, Texas Woman's University, Denton, Texas 76204

Texas Woman's University (TWU) initiated two butterfly gardens containing 90+ native plant species for pollinator conservation and sustainability education. These urban native gardens provide food and nesting sites for native bees and butterflies whose populations are declining. Pollen studies are carried on to establish plant-pollinators relationship networks and a pollen database. The goal of this study was to observe seed morphology and build a seed database to be added to the pollen database in the virtual TWU Herbarium. This is an ongoing project, but, so far, seeds from 12 species representing 6 plant families were collected from the butterfly gardens and observed with a Hitachi TM3030Plus scanning electron microscope. Pictures of seed surface ornamentations were taken at magnifications of 40-3,000x. *Liatris* seeds had one of the most interesting types seed morphology; cone-shaped with feathery pappus at the top which helps with seed dispersal by wind. Seed body had well defined lines with hairs from top to bottom and what seems to be round glandular hairs in the spaces between lines. The seed database will help scientists identify native plant seeds by providing them a visual online resource.

BUILDING A POLLEN DATABASE AND PLANT-POLLINATOR NETWORK OF INTERACTIONS USING SCANNING ELECTRON MICROSCOPY. MAFIA MAHABUB RUMPA, ADINA ZIDERMANIS and CAMELIA MAIER

Division of Biology, School of the Sciences, Texas Woman's University, Denton, Texas 76204

Pollination is a mutually beneficial process for plants and pollinators. Plants are cross pollinated and provide pollen, nectar, and other feeding and nesting resources to pollinators. Most crops are pollinated by multiple pollinators including species of bees, butterflies, beetles, flies, and other insects. Urban sprawling fragments native plant-pollinator habitats. However, urban pollinator gardens, as those initiated at Texas Woman's University, contribute to pollinator conservation for Monarchs and many other butterflies, bees, and native bumblebees whose populations are in decline. The goal of this project is to study the plant-pollinator relationships. The objectives are to build 1) a database of pollen morphologies using microscopy techniques and 2) a network of native plant-pollinator relationships based on field observations and pollen microscopy.

Using a Hitachi TM3030Plus scanning electron microscope, pollen collected from 65 plant species belonging to 21 plant families and 20 pollinators were observed at magnifications of 50X to 3,500X. Plants from the *Asteraceae*, *Fabaceae*, *Lamiaceae*, *Malvaceae*, *Onagraceae*, *Plantaginaceae*, *Acanthaceae*, and *Verbenaceae* families were mostly preferred for nectar feeding and/or pollen collection by Swallowtail, Fritillary, and Monarch butterflies, bumble bee, and honeybee pollinator species. The network of mutualistic plant-pollinator relationships was based on comparing and matching pollen images from plants and pollinators and completed with field observations. This research will offer data for restoration and conservation activities as well as advice to gardeners and farmers on plant resources they need to enhance both the pollinator populations and crop yields.

INTERMYOFIBRILLAR ULTRASTRUCTURAL CHANGES BETWEEN CONTROL, INTERMITTENT CLAUDICATION, AND CRITICAL LIMB ISCHEMIA PATIENTS. DYLAN WILBURN¹, EMMA FLETCHER², DIMITRIOS MISERLIS³, BERND ZECHMANN⁴, and PANAGIOTIS KOUTAKIS²

¹Department of Health, Human Performance, and Recreation, Baylor University, Waco, TX

²Department of Biology, Baylor University, Waco, TX

³Department of Surgery, University of Texas Health Science Center San Antonio, San Antonio, TX

⁴Center for Microscopy and Imaging, Baylor University, Waco, Texas 76706

Peripheral artery disease (PAD) is associated with

the obstruction of peripheral arteries impairing blood flow to limbs that can be classified into four categories: asymptomatic, claudication, critical limb ischemia, and acute limb ischemia. Of these four categories, the most common clinical manifestation of symptomatic PAD is intermittent claudication (IC), which is defined as exercise-induced pain caused by ischemia that is relieved with rest. Critical limb ischemia (CLI) occurs when blood flow is severely impaired during rest conditions and can require amputations of the compromised limb. During IC, it has been postulated that exposure to repeated cycles of ischemia and reperfusion insults can lead to a myopathy that progresses to further impair muscle function independent of hemodynamic obstruction (Pipinos et al., 2008). However, the structural changes that occur within the IC and CLI stages of PAD have not been well characterized and need further elucidation.

We aimed to assess changes in ultrastructure within the skeletal muscle intermyofibrillar region between control, IC, and CLI PAD patients. A total of 40 participants (15 control, 10 IC, & 15 CLI) were recruited to take part in this study. Muscle samples were collected from the gastrocnemius and immediately fixed in 2.5% glutaraldehyde phosphate-buffer solution. All samples were then washed 3 times for 10 min in phosphate buffer solution before secondary fixation in 1% osmium tetroxide (OsO₄) for 2 hr. Muscle samples were washed again 3 times for 10 min before undergoing dehydration in increasing acetone concentrations (50%, 70%, 90%, and 100%). Samples were embedded with increasing gradients (1:2, 1:1, 2:1) of Embed 812 before being completely immersed in 100% Embed 812 and polymerized at 60°C for 48 h. After sectioning (70 nm) thin sections, post-sectioning staining was completed by incubating grids with 2% uranyl acetate (15 min) and 1% lead citrate (5 min). Total relative mitochondria area, average mitochondrial cross-sectional area (CSA), mitochondria count per area, total relative myofibril area, average m-line length, Z-disc count per area, total relative lipid droplet area, average lipid droplet CSA, lipid droplet count per area, and total sarcoplasmic area were measured for each participant using two individual micrographs. All variables were statistically assessed using a one-way ANOVA with a Tukey post hoc or Kruskal Wallis with pairwise comparisons with a Bonferroni correction at significance of $p < .05$.

There was a significant decrease in the relative mitochondria area ($F=15.081$, $p < .001$) seen in CLI patients due to a decrease in total mitochondria count ($F=17.291$, $p < .001$) rather than average mitochondria CSA ($X^2=2.267$, $p=.322$) (Figure 1). There was no significant difference in relative myofibril area between groups ($F=1.249$, $p=.299$). However, there was a significant decrease in sarcomere M-line lengths ($X^2=9.067$, $p=.011$) seen in CLI patients when compared to controls ($p=.001$). No difference in M-line lengths was found between control and IC ($p=.513$) or IC and CLI ($p=.87$). No difference in Z-disc count was found between groups ($F=1.545$, $p=.227$). There was no difference found between groups for relative lipid droplet area ($X^2=.133$, $p=.936$), average lipid droplet CSA ($X^2=1.067$,

p=.587), or lipid droplet count ($X^2=.133$, p=.936). There was no significant difference in sarcoplasmic area between the groups ($F=1.25$, p=.298). Major structural alterations were found within the PAD conditions (Figure 2 B1-3) showing dramatically disorganized myofibril structure, sarcomere smearing, and Z-disc misalignment when compared to controls (Figure 2 A). These instances of structural damage were present in both IC and CLI but were much more prevalent in the CLI patients. The myopathy that develops within PAD patients dramatically affects mitochondria content and is most identifiable in later stages of the diseases.

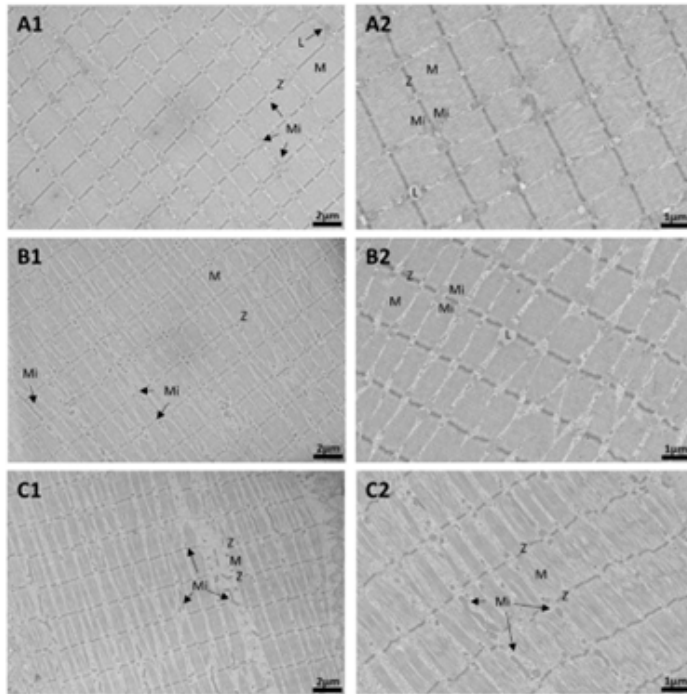


Figure 1: Representative images of ultrastructural changes that occur within the intermyofibrillar region of myofiber in control (A1-2), intermittent claudicants (B1-2), and critical limb ischemia (C1-2) peripheral artery disease patients. There is decreased mitochondrial (Mi) content in critical limb ischemia patients that is coupled with shorter sarcomere M-line lengths (M). The existing mitochondria within the critical limb ischemia patients appear elongated and are localized less frequently in pairs at Z-discs (Z) when compared to control participants (A1-2). There were no changes found between groups when assessing intramyocellular lipid droplet (L) indices.

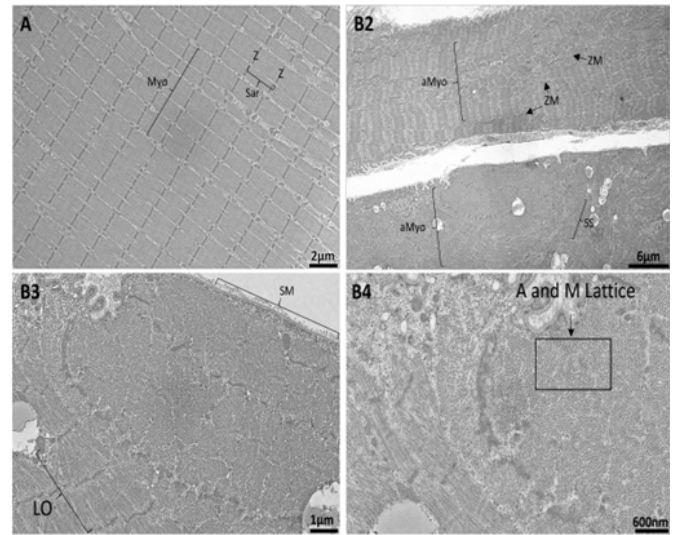
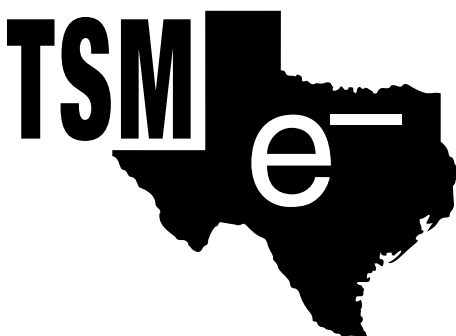


Figure 2: Disruption of the normally parallel striated myofibrillar (Myo) structure within a myofiber with PAD (B1-3) compared to control (A). In the upper myofiber in micrograph B2 there is sarcomere (Sar) smearing (SS), Z-disc (Z) misalignment (ZM) and abnormal myofibril organization that appears non-linear or parallel. In the bottom myofiber of B2 there is a representative image of abnormal formation of contractile apparatus (aMyo) that is 90° from the normal longitudinal orientation (LO) of the myofibrils. This is seen in some of the PAD patients both IC and CLI. In micrographs B3 and B4, a closer view of this region shows the actin (A) and myosin (M) hexagonal lattice structure (black box) that is only seen in anatomical cross-section. The presence of an undisturbed sarcolemma membrane (SM) suggest that this is not an artifact from tissue processing but possibly from myopathy within this patient population.

References:

- Pipinos, I.I., Judge, A.R., Selsby, J.T., Zhu, Z., Swanson, S.A., Nella, A.A., et al. (2008) The Myopathy of Peripheral Arterial Occlusive Disease: Part 1. Functional and Histomorphological Changes and Evidence for Mitochondrial Dysfunction. *Vasc Endovasc Surg*; 41(6), 481-9.
- Pipinos, I.I., Judge, A.R., Selsby, J.T., Zhu, Z., Swanson, S.A., Nella, A.A., et al. (2008) The Myopathy of Peripheral Arterial Occlusive Disease: Part 2. Oxidative Stress, Neuropathy, and Shift in Muscle Fiber Type. *Vasc Endovasc Surg*; 42(2), 101-12.



USING AUTOMATED SLIDE SCANNING AND CONFOCAL FLUORESCENCE MICROSCOPY TO UNCOVER PATHOLOGICAL MECHANISMS IN PSYCHIATRIC DISEASE STATES. JOHN TYLER O'BRIEN, SOPHIA JALILVAND, NEHA SUJI, AAMNA KHAN, ROHAN JUPELLY, YI LUO, SKYLAR MENDEZ, SIERRA, RODRIGUEZ, SANJANA TATA, KENDALL CULPEPPER, ZARA KANWAL, RIA NUNA, NAISHA VINAYAK, and SVEN KROENER

Diagnosing and treating psychiatric disorders is a major challenge due to the complex interplay of genetic, environmental, and epigenetic factors. To advance our understanding and develop targeted therapies, it is essential to identify the spatial and temporal boundaries from which neuropathological alterations emerge and coalesce into psychiatric phenotypes. Among the many laboratory techniques used to investigate the brain and behavior, microscopy is a critical tool in the field of biological research, enabling anatomical and physiological visualization at various levels of resolution. Here, we tour recent research in the Kroener Lab which applies slide scanning and confocal fluorescence microscopy, combined with viral-vector circuit tracing and quantitative immunohistochemistry, to uncover pathological mechanisms in rodent models of substance use disorders (SUDs). We also present novel findings from human postmortem studies of schizophrenic patients. These techniques and methodological approaches enable high-resolution analysis at the molecular, cellular, and circuit level, leading to a better understanding of aberrant cell-type and circuit-specific changes unique to psychiatric pathologies (Figures 1-2).

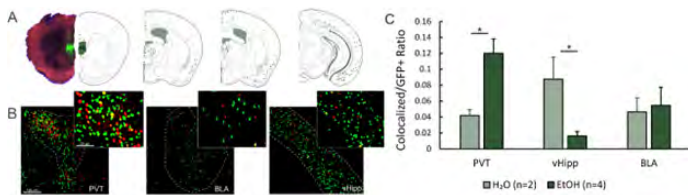


Figure 1: Distinct and overlapping neuronal ensembles provide information with temporal and spatial precision. A) Retrograde tracing of PFC networks was achieved by infusion of (green) adeno-associated virus (hSyn-GFP AAV Retro) into the mouse infralimbic (IL) PFC and major projection centers were mapped in coronal sections. B) GFP+ (green, IL-projecting neurons), cFos+ (red, activity-dependent marker), and colocalized (yellow, GFP+ and cFos+) neurons in the paraventricular thalamus (PVT), basolateral amygdala (BLA), and ventral hippocampus (vHipp) reveal circuit-specific alterations in response to ethanol seeking behavior. C) Quantifying the ratio of colocalized/GFP+ neurons in the PVT, vHipp, and BLA for mice self-administering for water or ethanol rewards.

The chronic relapsing cycle of drug addiction involves transitions between distinct stages of intoxication, withdrawal, and craving. Studies in animal models and human patients suggest that each of these stages are mediated by discrete neural circuits reinforced by drug-related cues and contexts that usurp neural processes involved in rewarded-related learning. A major behavioral

maladaptation associated with the development and maintenance of substance use disorders is a loss of response inhibition resulting from functional impairment of the prefrontal cortex (PFC). Using a rodent models of alcohol use disorder (AUD), we mapped synaptic inputs which converge on the PFC and identified functionally active circuits during distinct time points of the addiction cycle. Our results uncovered an alcohol-activated network that drives synaptic changes in the PFC. These findings reveal circuit-specific substrates that may lead to increased craving for drug rewards and higher risks of relapse (Figure 1).

Disruption of core cognitive processes, such as working memory impairments, are considered an integral part of the schizophrenia disease pathophysiology. Multiple lines of evidence link these cognitive disturbances to anomalies in cortical parvalbumin (PV)- expressing interneurons (PVIs). While the precise etiology of these changes remains uncertain, redox dysregulation and oxidative stress may be a pathophysiological convergence point in schizophrenia, causing dysfunction of GABAergic interneurons and loss of PV. Here, we show that the mitochondrial matrix protein cyclophilin-D (CypD), a critical initiator of the mitochondrial permeability transition pore (mPTP) and subsequent modulator of the intracellular redox state, may be involved in PVI alterations in schizophrenia. Using human dorsolateral prefrontal cortex (DLPFC) tissue, we measured PV and CypD expression levels in layer specific PVIs. Our results indicate that schizophrenia is characterized by lower PV expression in layers 2-4 compared to unaffected comparison subjects. These laminar-specific PVI alterations were reciprocally linked to significant elevations in CypD. Taken together, our findings implicate CypD-mediated mPTP formation as a potential contributor to PVI deficits and cognitive dysfunction in schizophrenia (Figure 2).

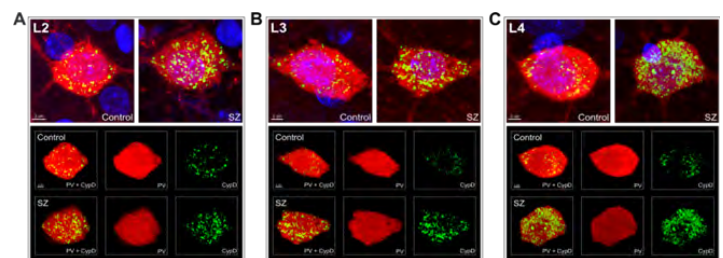


Figure 2: Quantifying mitochondrial redox states in schizophrenia with laminar- and cell-type specific resolution. High magnification (100X) fluorescent microscopy images of parvalbumin interneurons (red) co-labeled with markers for oxidative stress (green, cyclophilin-D protein) and nuclear DNA (blue, DAPI). For subjects with schizophrenia, parvalbumin (PV) intensity significantly differed across layers, creating a superficial-deep gradient of declining PV intensity in layers II (A), III (B), and IV (C) which were reciprocally linked to significant elevations in cyclophilin-D (A-C).

ANALGESIC EFFECT OF *EUPHORBIA BICOLOR* IN RAT SPINAL CORD BY CONFOCAL MICROSCOPY.
TEMILOLUWA P. OLAOLUWA, ANUSHA ADHIKARI, CAMELIA MAIER, and DAYNA L. AVERITT

Division of Biology, School of the Sciences, Texas Woman's University, Denton, Texas 76204

Pain associated with burn injuries has been linked to nociceptor sensitization and can lead to chronic pain. Current treatment for burn pain includes analgesics such as non-steroidal anti-inflammatory drugs, opioids, and gabapentinoids, all linked to undesirable side effects. As burns represent a particularly challenging type of injury to treat, novel strategies that mitigate burn pain are needed. Our previous studies indicate that the latex extract of *Euphorbia bicolor*, a plant native to the south-central United States, may contain phytochemicals that could serve as a novel analgesic(s). Adult male Sprague-Dawley rats (200-300 g) received a full thickness thermal injury to the plantar surface of the right hind paw by applying a soldering iron tip at 100°C for 30 seconds. Two concentrations of *E. bicolor* ethanol latex extract, 100 µg/mL and 500 µg/mL, in 0.9% sterile saline were delivered as local injections into the burn-injured paw. At week 3, the rats (n=12) were perfusion fixed with 4% paraformaldehyde and spinal cord (L2-L5) was extracted in 30% sucrose and cryosectioned. Fluorescent immunohistochemistry was performed on 30 µm sections of spinal cord using primary antibodies against calcitonin gene-related peptide (rabbit anti-CGRP; 1:1000) and neurofilament heavy NF200 (chicken anti-NF200; 1:1000). Tissues were then incubated in goat anti-rabbit 568 or goat anti-chicken 488 Alexa Fluors (1:300) and visualized with a ZEISS LSM confocal microscope. Peripheral analgesia was detected within 72 hours of *E. bicolor* extract injection at the injured paw with both the 100 and 500 µg/mL doses and analgesia was significant for up to three weeks. Rats displaying *E. bicolor* extract-evoked analgesia had significantly reduced immunoreactivity of the pronociceptive peptides calcitonin gene related peptide (CGRP) in the lumbar dorsal horn of the spinal cord. Our analysis of the lumbar spinal cord indicates that *E. bicolor* phytochemicals reduce pronociceptive peptides in the dorsal horn, which receives sensory afferent input from the Dorsal Root Ganglion (DRG). This data indicates that *E. bicolor* phytochemicals reduce burn pain partly by reducing pronociceptive peptide release from sensory afferents at the spinal cord.



SEXUAL DIMORPHISM CHANGES GLANDULAR TRICHOME DENSITY AND KARYOTYPE IN *CANNABIS SATIVA* L. ALONG WITH CANNABINOIDS CONTENT. ANINDITA DAS¹, TAYLOR RANGEL^{2*}, NABARUN GHOSH², SATYA NARAYAN JENA¹, and ANATH BANDHU DAS³

¹Plant Genetics Resources and Improvement, CSIR-National Botanical Research Institute, Rana Pratap Marg, Lucknow-226001, U.P, India

²Department of Life Earth and Environmental Sciences, West Texas A&M University, Canyon, Texas, USA

³Molecular Cytogenetics Laboratory, Department of Botany, Utkal University, Vani Vihar, Bhubaneswar 751004, Odisha, India

Cannabis sativa L. belongs to the family *Cannabaceae* and is widely distributed in Central Asia including Turkestan, Pakistan, South China and Himalayas (Wills, 1998). It is one of the major sources of medicine, oil, and fiber, and is cultivated as a cash crop in many countries (Lavery et al., 2019). For long time, it has been used in medicine for treating pain, nausea, depression, glaucoma, asthma, and insomnia. The medicinal properties of this species are attributed to the two major active compounds, namely δ -9-tetrahydrocannabinol (THC) and cannabidiol (CBD) (Figure 1 A, B). (Mechoulam et al., 1976; Duke and Wain, 1981). When using a high enough dose of CBD from *Cannabis*, the CBD can inhibit the Corona virus protein from binding to (ACE2) and transmembrane serine protease 2 (TMPRSS2); thus, it can be used as prophylaxis treatment to prevent SARS-CoV-2 infection (Ragia and Manolopoulos, 2020).

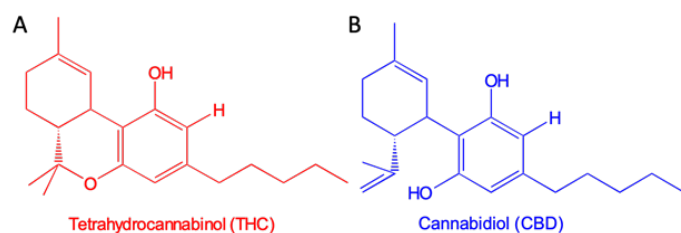


Figure 1. Chemical structure of the two major active compounds in *Cannabis sativa*: A) δ -9-tetrahydrocannabinol (THC) and B) Cannabidiol (CBD).

We performed the Micro-Raman-spectrometric analysis of THC and CBD and the obtained results corroborated with the quantum chemical simulated Raman spectra of their acid-forms: tetrahydrocannabinol acid (THCA) (Figure 1A) and cannabidiol acid (CBDA) (Figure 1B). *In vitro* assessment of cannabinoid content revealed that there is a significantly higher amount of THC than CBD in female plants.

There are previous reports on the ontogeny and structural organization of the matured trichomes (Briosi and Tognini,

1894; Ram and Nath 1964). Light and Scanning Electron Microscopy were used to characterize the trichomes to aid the forensic identification of illegal *Cannabis* products (Ledbetter and Krikorian, 1975; Dayanandan and Kaufman 1976; Hammond and Mahlberg, 1977). The reports on the studies of trichome morphoanatomy in relation to sexual dimorphism, chromosomal structure and cannabinoids content of *Cannabis sativa* L. (Figure 2A). Sexual dimorphism is very conspicuous in *Cannabis* sp. with prominent differentiating characters visible in the female (Figure 2B) and male plant (Figure 2C). A significant variation in the leaf surface topography in terms of glandular trichomes (Figure 2D) density were noted. From the numerical assessment, we can conclude that the glandular sessile and bulbous trichomes (Figure 2D) were distributed in a much higher number in the female plants compared to the male plants (Figures 2 E and F). SEM studies revealed that the size variation of glandular sessile trichomes was significant between the male and female plants. We observed the cystolith trichomes and slender covering trichomes were distributed primarily on the adaxial surface, while the covering trichomes occurred only on the abaxial surface of the leaf (Figure 2G); however this attribute was common among the male and female plants (Figures 2H and I). Anatomical studies (Figures 2 J, K, L, M) of the leaf also confirmed that the cystolith crystals of calcium carbonate and cluster crystals of calcium oxalate were found to be distributed on the leaf surface. Comparative analyses of karyotype and karyotypic asymmetry confirmed that the diploid set, $2n=20$ chromosomes were composed of: $2n=8m+10sm+XX_{nsm}$ and $2n=8m+10smX_{nsm}Y_{nm}$ in the female and male plants respectively. X chromosome long arm length was higher compared to the Y chromosome in male plants. Flow cytometry analysis revealed the genome size of 2C DNA content of ~820.12 Mb in female and 845.23 Mb in male plants (Figures 2N and O).

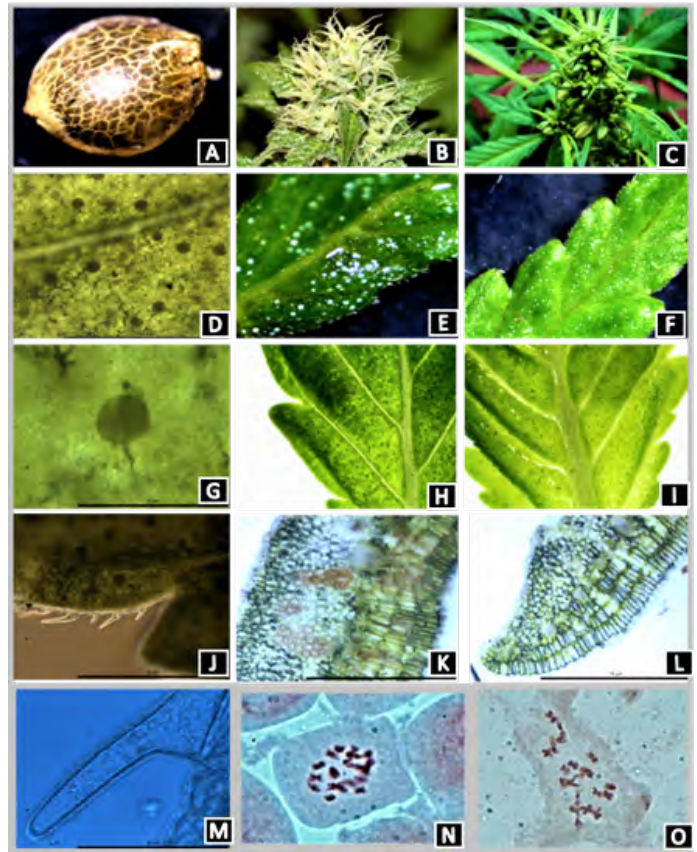


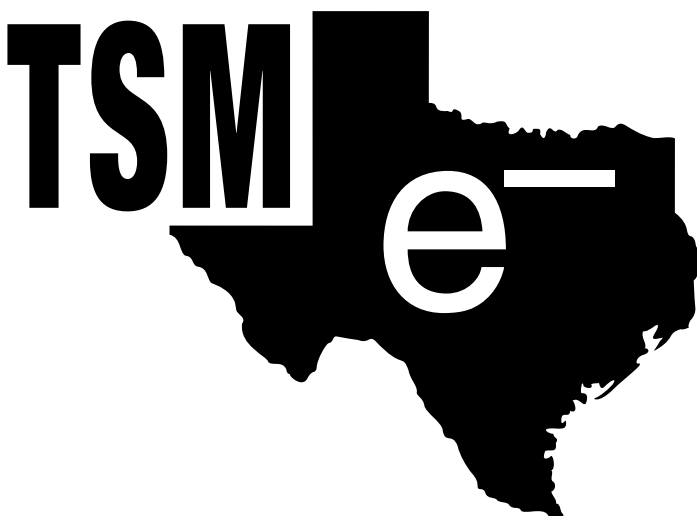
Figure 2. Morpho-cytological features of female and male *Cannabis sativa* L. (A) seed, (B) female and (C) male plant with inflorescence, (D) glandular trichome on leaf surface of (E) female and (F) male plant, (G) bulbous glandular trichome (H-I) trichome on leaf surfaces; (J-K) leaf anatomy showing gland on (J) female and (K) male plant; (L-M) leaf surface slender covering trichome magnified view; (N-O) somatic metaphase chromosome $2n=20$ in (m) female and (n) male plant.

It is important to collect and index the natural genetic varieties and develop inbred lines through sibling breeding to produce genotypes with increased cannabidiol content and reduced tetrahydrocannabinol. This study is important to better understand the *Cannabis* micro-morphology, cytogenetics and in situ quantification of THC and CBD for developing the desired clonal variant of the species for effective medical uses.

Plant biotechnology, genomics and clonal selection via plant breeding will aid in optimizing phyto-cannabinoid synthesis to create plants with desired phyto-cannabinoid profiles, from zero THC hemp to novel phyto-cannabinoids for medicinal uses.

References:

- Brioso, G., Tognini, F. (1894). Intorno alla anatomia della canapa (*Cannabis sativa* L.). *Atti Ist Bot Pavia* 3:91–209.
 Dayanandan, P., Kaufman, P. B. (1976). Trichomes of *Cannabis sativa* L. (*Cannabaceae*). *Am J Bot* 63:578–591.



Duke, J., Wain, K. (1981). Medicinal plants of the world. Computer index with more than 85000 entries. Handbook of Medicinal Herbs. Edited by J.A. Duke. CRC Press, Boca Raton, Fla. Pp. 96.

Hammond, C. T., Mahlberg, P. G. (1977). Morphogenesis of capitate glandular hairs of *Cannabis sativa* (*Cannabaceae*). *Am J Bot* 64:1023–1031.

Laverty, K.U., Stout, J.M., Sullivan, M.J., Shah, H., Gill, N., Holbrook, L., et al. (2019). A physical and genetic map of *Cannabis sativa* identifies extensive rearrangements at the THC/CBD acid synthase loci. *Genome Res.* 29: 146–156. doi:10.1101/gr.242594.118.

Ledbetter, M. C., Krikorian, A. (1975). Trichomes of *Cannabis sativa* as viewed with scanning electron microscope. *Phytomorphology* 25:166–176.

Mechoulam, R., Lander, N., Dikstein, S., Carlini, E., Blumenthal, M. (1976). On the therapeutic possibilities of some cannabinoids. In *The Therapeutic Potential of Marijuana*. Edited by S. Cohen and R.C. Stillman. Springer. pp. 35–45.

Ram, H.M., Nath, R. (1964). The morphology and embryology of *Cannabis sativa* Linn. *Phytomorph* 14:414–429.

Ragia G., Manolopoulos V.G. (2020). Inhibition of SARS-CoV-2 entry through the ACE2/TMPRSS2 pathway: A promising approach for uncovering early COVID-19 drug therapies. *Eur. J. Clin. Pharmacol.*; 76:1–8. doi: 10.1007/s00228-020-02963-4.

Wills, S. (1998). *Cannabis use and abuse by man: a historical perspective*. Harwood Academic, Amsterdam.

MATERIAL SCIENCES Spring 2023

WHAT CAN SCANNING ELECTRON MICROSCOPY TELL US ABOUT THE POTENTIAL HEALTH IMPACTS OF UNCONTROLLED COAL FIRES?

HENRY R. DODDS and ROBERT B. FINKELMAN
The Geosciences Department, School of Natural Sciences and Mathematics, University of Texas at Dallas, Richardson, TX, 75080

Uncontrolled coal fires present a unique and significant risk to the health of the environment and to the people working and living nearby. Large, hot fires, along with smoke containing a myriad of toxic chemicals can burn the valuable coal resource, threaten the wildlife, and all while polluting the atmosphere, plants and waters of the area. A long-lived and still burning coal fire in Jharia, India exists in the middle of active coal mining operations and is surrounded by populated villages. The people of the area show an unusual concentration of health complications. A sample of solid condensate from around a smoke vent was collected and studied using Scanning Electron Microscopy (SEM) and revealed numerous solid phases with exotic chemistries.

Potentially hazardous chemicals such as NH₄, F, Cl, Pb, Cd, As, Se, and S were found, in complex phase relationships and crystal growth patterns.

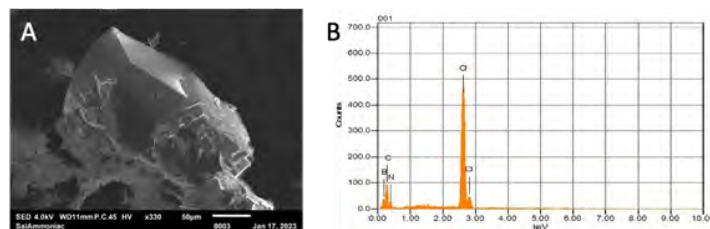


Figure 1: SED photomicrograph of a crystal of Ammonium Chloride with apparent Boron (A). Point EDS spectrum (B). Carbon present is likely due mostly to C sputter coating on sample.

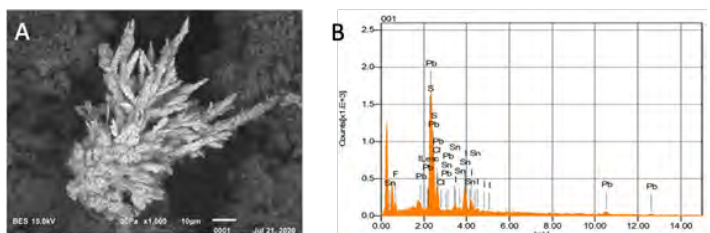


Figure 2: SED photomicrograph of Lead and Tin halide crystals (A). Point EDS spectrum (B). Leftmost peak is Carbon from sputter coating.

Using electron microscopy (backscattered and secondary electron modes) and an energy dispersive X-ray detector to study the phases present in the condensate can illuminate what health risks are posed to the people living and working around this fire.

CHARACTERIZATION OF MICROSCOPIC PARTICLES DISPERSED IN LUBRICATING AUTOMOTIVE GREASES USING SCANNING ELECTRON MICROSCOPY AND ENERGY DISPERSIVE X-RAY SPECTROSCOPY. JARED ESTEVANES, PATRICK BUZZINI and GERALDINE MONJARDEZ

Department of Forensic Sciences, Sam Houston State University, Texas, 77340, U.S.

In the context of a forensic case, lubricating automotive greases may be submitted to a laboratory for identification as general unknowns, may be recovered from the garments of a suspect allegedly involved in events under investigation, or they may be found as stains on the ground at an automotive accident scene. Numerous studies have been conducted differentiating automotive motor oil for forensic applications, however, little research has been conducted to characterize or differentiate lubricating automotive greases. Investigating the physical and chemical properties that allow a reliable identification and differentiation of greases could help forensic laboratory personnel provide information to further investigations and assist law enforcement in the solving of crimes involving vehicles.

Microscopic examinations previously conducted on this subject in the context of a master theses research at Sam Houston State University (Day, 2018 and Estevanes, 2021) showed the presence of microscopic particles dispersed in pure automotive greases that were part of the original formulation of the grease samples. Three particle types were identified and consequently classified by their optical properties as opaque, isotropic, and anisotropic. These particles differed considerably between different grease samples. It was discovered that the opaque particles analyzed were solid lubricant additives within the greases and these particles displayed potentially discriminating properties.

Previous attempts to characterize the isotropic and anisotropic particles with Scanning Electron Microscopy-Energy Dispersive X-ray Spectroscopy (SEM-EDS) proved challenging compared to the opaque particles. The objectives of this research were to determine the optimal sample preparation and operating parameters of the SEM-EDS to successfully select and characterize the isotropic and anisotropic particles, as well as gaining a deeper understanding of how the morphology and/or elemental composition of these different particles relate to their challenging analysis.

An extraction procedure using D-limonene was used to remove the particles from the grease matrix. Light microscopy was then used to confirm that the isotropic and anisotropic particles of interest were left intact after the extraction process. The extracted residues were then analyzed using SEM-EDS to determine the particle elemental composition. Variable pressure SEM was used to reduce interference effects with a pressure of 60 Pa. Targets for EDS analysis were then selected based upon backscatter images and particle morphology.

The isotropic and anisotropic particle sizes and morphologies differed among the sample sets, with no patterns observed when taking into consideration the greases' end use. Particle sizes were small, usually less than 5 μm , and possessed mostly spherical shape. EDS revealed isotropic and anisotropic particles contained lighter elements, such as calcium and sulfur, which contrasts to the heavier elements identified for the opaque particles. These chemical differences of the particles, combined with microscopic information, display potentially discriminating properties for automotive greases.

This study demonstrates the potential differentiability of automotive greases based upon their microscopic and chemical characteristics. This information expands the consideration of new types of trace materials to automotive greases and show their potential contribution to forensic investigations.

References:

Day, J. (2018). The Characterization and Discrimination of Transmission Fluids, Brake Fluids, and Vehicular Greases [Unpublished master's thesis]. Sam Houston

State University.

Estevanes, J. (2021). Characterization of Automotive Greases via Scanning Electron Microscopy/Energy Dispersive X-Ray Spectroscopy [Unpublished master's thesis]. Sam Houston State University.

CHARACTERIZATION OF EJECTED PARTICLES FROM A LITHIUM-ION BATTERY DURING THERMAL RUNAWAY. CHRISTIAN A. LANDRY, PAUL O. ADEFIRANYE, SAMUEL A. MCCAULLEY, and JAMES C. THOMAS

J. Mike Walker '66 Department of Mechanical Engineering, Texas A&M University, College Station, Texas, 77845

The recent influx of the integration of lithium-ion batteries (LIB) in technology has led to a rising concern regarding their safety. The failure of LIBs via thermal runaway (TR) can occur due to many different onsetting phenomena (physical, thermal, electrical, etc.) and may cause the battery to catch fire and combust. During the TR process, the combustion process produces a variety of hazards including significant energy release, jet flames, release toxic and/or secondarily combustible gases, and production of micro- and nano-particulates. In the current study, the ejected particulates are analyzed via microscopy and materials analysis methods. The goal of this research is to understand the extent of the combustion reaction taking place within the LIB during TR. A single Panasonic NCR 18650B cell at 100% state-of-charge (SoC) was heated to TR under ambient conditions and in air. Ejected particulates were safely collected and prepared for microscopy and further analyses. Scanning electron microscopy (SEM) and energy dispersive spectroscopy (EDS) techniques were first utilized to investigate particulate sizing and elemental composition. A representative group of collected particles is shown in Figure 1 which includes a more detailed EDS analysis of a single particle. A wide range of particle sizes (< 1 μm – 2 mm) and shapes were observed throughout the sample. The EDS elemental mapping approach allowed for a visualization of the different elements present in the small particulate. The particulate contains a variety of constituent elements, and the mapping analysis indicates it is a chunk from a single layer of the battery's internal jelly roll. More explicitly, it contains clear traces of the anode (Carbon), cathode (Nickel, Cobalt, and Iron), and current collectors (Al or Cu). In addition, it contains some elements from the electrolyte solution (i.e., Phosphorous), but not others (i.e., Fluorine). Elements belonging to each constituent part (e.g., anode, cathode, etc.) are observed to have mixed and reacted together. The presence of oxygen throughout the entire particle indicates all components have at least partially reacted with the ambient air, as well. A second representative particle belonging to the anode is shown in Figure 2 where the point and scan

EDS approach was applied to understand the elemental composition of surface-level features. A strong variation in the elemental composition is observed, but a high concentration of oxygen is observed in all the particles examined. Further analyses with x-ray powder diffraction (XRD) and x-ray photoelectron spectroscopy (XPS) have been conducted to elucidate the molecular composition of crystalline components and the type of molecular bonds present, respectively, but these are not shown here for brevity. These analyses also provide crucial information about the presence and concentration of lighter elements (i.e., Hydrogen and Lithium) which are difficult to accurately detect with EDS analyses. Preliminary XRD analyses indicate that the ejected particles contain a wide variety of single- and mixed-metal compounds which are all fully or partially oxidized. A low-resolution XPs scan illustrated similar results as the EDS analyses, but demonstrated the presence of Hydrogen, Lithium, and some contaminants traced to the heating system (Tin and Silicon). These key findings from our study will be useful in further experiments which will seek to follow similar microscopic analyses for batteries with different compositions at different SoCs. The findings will prove integral to the development of safer LIBs and give a fundamental understanding of the reactions taking place during TR.

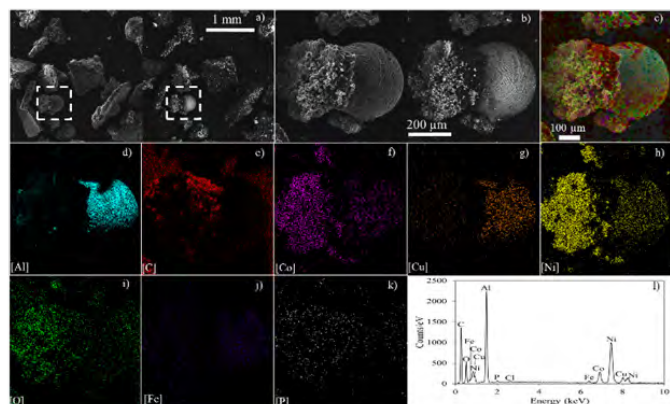


Figure 1: SEM images of particulate ejecta with corresponding EDS mapping analyses for visualization of elemental dispersion from a LIB which underwent TR.

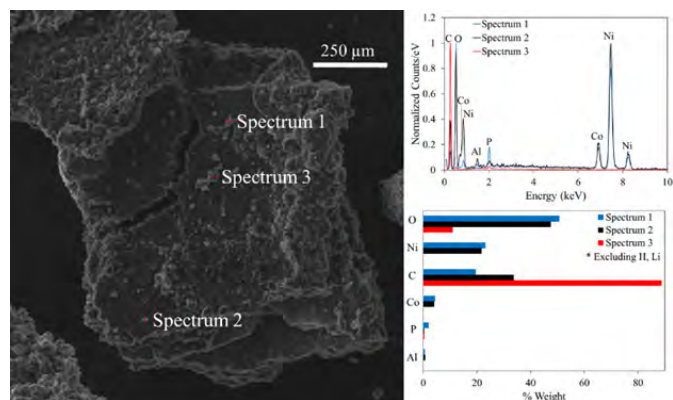


Figure 2. SEM image of particulate ejecta with corresponding EDS point analyses for visualization of elemental dispersion from a LIB which underwent TR.

ENCAPSULATION OF SPIONs IN THE CORE OF WRINKLED MESOPOROUS SILICA. A. K. M. NUR ALAM SIDDIKI and KENNETH J BALKUS JR.

Department of Chemistry and Biochemistry, University of Texas at Dallas, TX 75080, USA

Wrinkled mesoporous silica is a type of porous silica material featuring cone-shaped pores formed by a wrinkled structure. This material can be fabricated with different morphologies and pore structures. By encapsulating Superparamagnetic Iron Oxide Nanoparticles (SPIONs) in wrinkled mesoporous silica, it becomes possible to develop its potential in various imaging, plasmonic, and photothermal applications. In this study, a convenient method for the encapsulation of SPIONs in the core of wrinkled mesoporous silica is reported. SPIONs were synthesized via a reduction-precipitation method and were subsequently encapsulated in the core of wrinkled mesoporous silica using a surfactant template during synthesis. The resulting material was characterized using transmission electron microscopy (TEM), scanning electron microscopy (SEM), UV-Vis spectroscopy, Physical Property Measurement System (PPMS), and X-ray diffraction (XRD).

The particle size distribution of the SPIONs were calculated from TEM images using ImageJ. TEM images of the encapsulated particles show that the wrinkled structure effectively encapsulates the SPIONs within the core, without any detectable presence of the SPIONs in the outer mesopores. SEM imaging reveals that the pores have a conical shape and wide openings. The encapsulation of SPIONs within wrinkled mesoporous silica offers several advantages, such as protection against oxidation, enhanced dispersibility and colloidal stability, and a surface for drug molecule conjugation and targeted delivery.

ADVANCED E-BEAM LITHOGRAPHY FOR FABRICATION OF ELECTRICAL CONNECTIONS TO TEST RELIABILITY OF METALLIC NANOWIRES.

M. WALIULLAH, and R. A. BERNAL

Department of Mechanical Engineering, The University of Texas at Dallas, Richardson, TX 75080

In today's technology industry, the transistors and interconnects have reached such a small size (5 nm) that it is becoming impossible to shrink them further. As a result, the industry is leaning towards functionalized devices rather than miniaturized ones e.g., flexible electronics, wearable electronics etc. Metallic nanowires have excellent electrical, mechanical, and optical properties appropriate for the emerging technologies mentioned above (Song et al., 2014). However, in the nanoscale, phonon scattering and grain boundary diffusion become more and more significant. Hence, for a successful application in electronic devices, assessing the structure-function relationship of individual nanowires, from an electrical reliability perspective, is required.

Commercially available metallic nanowires e.g., silver and gold nanowires have a special type of grain boundaries called penta-twins. In our lab, we have synthesized another type of twin boundary structure called transverse twins for gold nanowires. We are investigating the structure-function relationship for penta-twinned silver nanowires (Joule heating due to phonon scattering) and both type of twins for gold nanowires (Electromigration through twin boundaries of different orientations).

For these investigations, we needed to connect individual silver and gold nanowires with an external circuit. The connections were fabricated in two layers—firstly, leads connecting randomly deposited sub-100 nm nanowires, fabricated by e-beam lithography (EBL) (Figure 1) and secondly, gold pads, connecting to the leads, fabricated by photolithography (Figure 2). The pads were wirebonded to a pin grid array and connected to a PCB and switch system to test each nanowire until failure. In this fabrication work, we faced a lot of challenges which include deterioration of nanowires under O₂ plasma, their incompatibility with adhesion layer in metal deposition, breaking of EBL pattern due to contaminants in gold nanowire solution, higher contact resistance due to faster deposition rate in e-beam evaporation, to list a few. We solved these problems and achieved successful electrical connections to test electrical reliability of metallic nanowires.

After the electrical connections were established, the behavior of current density at failure for penta-twinned silver nanowires were characterized and plotted against diameters ranging from 53 nm to 173 nm, for 93 samples. Heat-transfer modelling was performed to compare with the experimental data, and Weibull statistics were used to quantify failure probabilities.

Some scatter was observed in the measurements which can be attributed to surface-roughness variations among samples, and variations in a polymer layer which comes as a by-product of the nanowire synthesis. These results quantify the Joule-heating electrical reliability of silver nanowires and highlight the importance of heat transfer in increasing it (Waliullah and Bernal, 2022).

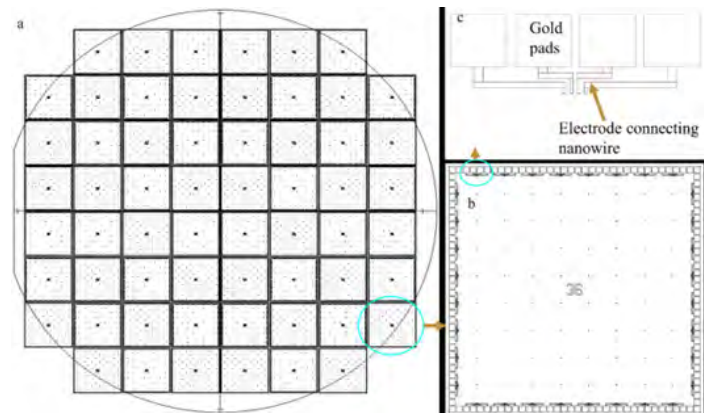


Figure 1. : Single nanowires connected with two leads. a. overview pictures showing the e-beam lithography lines connecting the nanowires with the photolithography traces. b. detail of a connected silver nanowire.

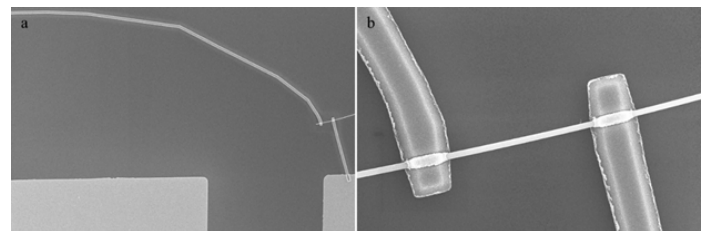


Figure 2: a. Design of the mask for a whole wafer, b. Details of a single chip, c. Details of a nanowire-connection site.

For gold nanowires, literature suggests that the orientation of twin boundaries play a big role in preventing atomic diffusion and hence, preventing an electrical failure mode called electromigration, which is governed by atomic diffusion. In this work, we are characterizing electromigration failure of gold nanowires for penta-twinned and transversely twinned gold nanowires, which allow electrical current along and across the twin boundaries respectively. The data obtained at different temperatures will reveal the structure-function relationship between the twins and electromigration failure mode and thus provide guideline to the flexible electronics industry.

References:

- Song, T.B. et al., (2014) "Nanoscale Joule Heating and Electromigration Enhanced Ripening of Silver Nanowire Contacts," *ACS Nano*, vol. 8, no. 3, pp. 2804–2811.
- Waliullah, M. and Bernal, R.A. (2022) "Current density at failure of twinned silver nanowires," *Nanotechnology*, vol. 33, no. 30, p. 305706.

DIRECT OBSERVATION OF THE CRYSTAL-MELT INTERFACE OF THE NDCE FEB MAGNET VIA *IN-SITU* ANNEALING & QUENCHING STEM.
XIANGYU ZHU¹, QINGXIAO WANG¹, LI SHAN³,
 BYUNG OH JUNG², MYUNGSHIN CHOI², SUNYONG
 SONG², SEOK NAMKUNG², NAMSEOK KANG², HUI-
 YOUN SHIN², MINHO JOO², XIANMING DAI³, and
 M.J. KIM¹

¹Department of Materials Science and Engineering;
²Materials & Devices Advanced Research Institute, LG
 Electronics, Seoul, 07796, KOREA

³Department of Mechanical Engineering University of
 Texas Dallas, Richardson, TX, 75080

Direct observation of the reaction interface is significant to establish the fundamental understanding of the evolution mechanism and facilitate the development of process engineering of the Rare Earth (RE)₂Fe₁₄B type magnets. Among these, elemental diffusion, oxidation, and phase transformation at high temperature are the major thermally induced responses that build the microstructure, and further govern the performance of (RE)₂Fe₁₄B type magnets. This work investigated the crystal-melt interface of the (Nd_{0.75}Ce_{0.25})₂Fe₁₄B magnets phase. Both the focused ion beam and *in-situ* STEM experiment are delicately designed to achieve the observation of both oxygen-involved and oxygen-free reaction dynamics within one specimen. (Figure 1)

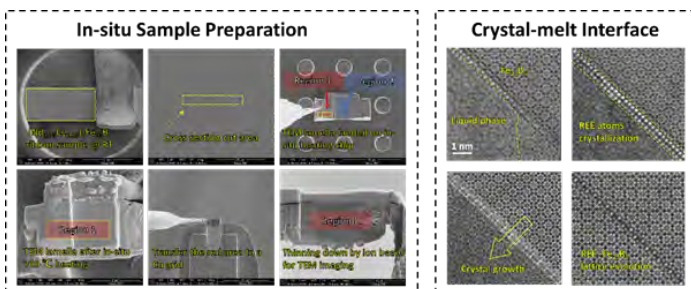


Figure 1: *In-situ* sample preparation & Crystal-melt Interface.

Remarkably, the reaction dynamics and interface structure between the liquid phase and the Fe₂₃B₆ metastable phase are clearly illustrated at atomic scale, providing compelling evidence for the early crystallization process of the NdCeFeB phase. The presented work also demonstrated that combining advanced FIB technique with *in-situ* annealing and quenching STEM is a powerful tool for investigating high-temperature reaction mechanisms and interface phenomena of complex systems.

SYNTHESIS OF COPPER OXIDE NANOSTRUCTURES BY ELECTRIC FIELD-ASSISTED PULSED LASER ABLATION IN WATER.
T. HESABIZADEH^{1,2} and G. GUISBIERS¹

¹ Department of Physics and Astronomy, University of
 Arkansas at Little Rock, Little Rock, AR 72204

² Department of Biology, University of Arkansas at Little
 Rock, Little Rock, AR 72204

Transition metal oxides such as cupric and cuprous oxides are strongly correlated materials made of Earth-abundant chemical elements displaying energy bandgaps around 1.2 and 2.1 eV. The ability to design nanostructures of cupric and cuprous oxide semiconductors with *in-situ* phase change and morphological transition will benefit several applications including photovoltaic energy conversion and photoelectrochemical water splitting. Here, we have developed a physico-chemical route to synthesize copper oxide nanostructures enabling the phase change of cupric oxide into cuprous oxide by using an electric-field of 10⁵ V/m in deionized water (DI); via a new synthetic design protocol called Electric-Field Assisted Pulsed Laser Ablation in Liquids (EFA-PLAL). The morphology of the nanostructures can also be tuned from a sphere of ~ 20 nm to an elongated leaf of ~ 3 μm by controlling the intensity of the applied electric field. Futuristically, the materials chemistry occurring during the EFA-PLAL synthesis protocol developed here can be leveraged to design various strongly correlated nanomaterials and heterostructures of other 3d transition metal oxides.

***IN VITRO* INHALATION TOXICOLOGY OF FINE PARTICLE AEROSOLS.**
JAMES LIU¹, SAHAR
 PRADHAN¹, BERND ZECHMANN², and CHRISTIE
 SAYES¹,

¹Department of Environmental Science, Baylor
 University, Waco, TX,

²Center for Microscopy and Imaging, Baylor University,
 Waco, TX.

Globally, an estimated 3.5 million annual deaths are attributed to fine particle exposure. Despite the alarming scale of the air pollution crisis, existing methods to assess inhalation toxicology are high-cost, low-throughput, and challenging to standardize. We are developing an *in vitro* framework based on streamlined aerosol characterization, exposure to relevant models, and collection of biological and biophysical endpoints. Innovative aspects include a custom-built exposure chamber (the Aerosol Exposure Surfactometer or AESM), the generation of dry particle aerosols, exposure at the air-liquid interface, and the use of lung surfactant as a biophysical model. Five particle types (aluminum, aluminum oxide, diesel exhaust, carbon nanotubes, and colloidal silica) were chosen for human

health relevance and to represent different physiochemical properties. Size, morphology, and surface charge were assessed with microscopy techniques (3D laser, scanning electron, transmission electron, atomic force) and dynamic light scattering. Microscopy was critical to identify size/shape heterogeneity and surface characteristics relevant to interactions with cells and surfactant. Aerosol size distribution and dose were measured with aerosol particle sizers and a quartz crystal microbalance. After exposure, the viability was measured for lung cells (A549) cultured at the air liquid interface. Surface tension was measured for lung surfactant after exposure. Diesel exhaust and silica were identified as potential threats to human health through both cytotoxicity and surfactant inhibition. Future work includes more sophisticated coculture models, improvements to the AESM, and analysis of mixtures interactions. This work builds a foundation for the high-throughput screening of aerosols that are potential hazards to human health.

SEM CHARACTERIZATION OF TI-TA-SN METALLIC FOAMS BY THE SPACER METHOD WITH 30% POROSITY FOR BIOMEDICAL USE. ABRAHAM MEJIA¹, ANDRES BEJAR¹, CLAUDIO AGUILAR², GEORGINA TORRES¹, ISMELI ALFONSO³, JOSE SOLIS⁴ and VICTOR AUGUSTO⁴.

¹División de Posgrado de Ingeniería Mecánica, Universidad Michoacana de San Nicolás de Hidalgo, Morelia, Michoacán de Ocampo, México

²Departamento de Ingeniería Metalúrgica y Materiales Universidad Técnica Federico Santa María, Valparaíso, Valparaíso, Chile

³Instituto de Investigaciones en Materiales, UNAM, Morelia, Michoacán de Ocampo, México.

⁴División de Estudios de Posgrado, Instituto Tecnológico de Tlalnepantla, Tlalnepantla de Baz Estado de México, México.

The use of titanium in biomedical applications has been successful due to its magnificent mechanical properties. In the following work, the microstructure and porosity of a Ti-Ta-Sn alloy metal foam with 30% spacer was evaluated by scanning electron microscopy (SEM). The purpose of this project is to develop a lightweight foam that acquires a better elastic modulus and elastic limit close to that of human bone (~30 GPa) (Aguilar et al., 2020; Geetha et al., 2009). For the manufacture of the foam, there are different methods, depending on the method used, the type of porosity will be favorable to obtain the following mechanical properties: high resistance to corrosion, toughness, hardness and resistance to wear. Open porosity fabrication can be homogeneous and promotes osseointegration and cell adhesion in biomaterials (Aguilar et al, 2020, Geetha et al, 2009, Ryan et al., 2006). Ti has a low modulus of elasticity and fatigue resistance in the β phase, CCC (>882 °C), while it offers good creep resistance when it presents an α phase,

hcp (<882 °C) (Mejia et al., 2022). The elaboration of the metallic foams was carried out by powder metallurgy to achieve the desired microstructure, for a cylindrical sample of 8 mm x 8 mm. In this case, ammonium bicarbonate was used as a spacer, the powders were 75% v/v of titanium, 13% v/v of tantalum and 12% v/v of tin, to each of the powders the percentage of the ammonium bicarbonate to obtain 100% accurate weighing. The powders were mixed for 30 minutes at 30 Hz using the principle of impact-friction grinding, the already mixed powders were deposited in a cylindrical die of 8 mm diameter steel, compacted at 430 MPa. To obtain the 8 mm long green sample, it was subsequently sintered in a conventional furnace with a controlled temperature with an argon atmosphere and a temperature curve from 25 °C to 800 °C; after 120 minutes it was increased to 800 °C up to 1200 °C. Cooling from 1200 °C to 100 °C was carried out by lowering the temperature by 3°C per minute.

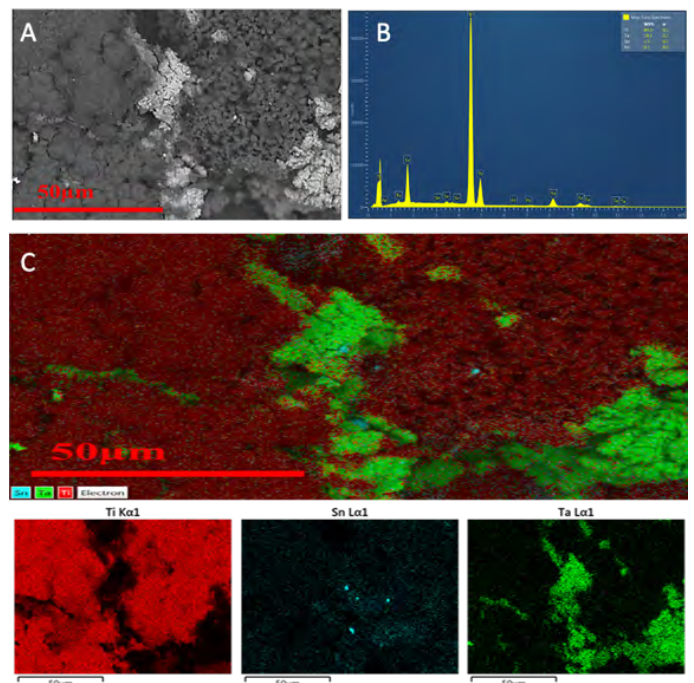


Figure 1: SEM characterization of Ti-Ta-Sn metallic foams. Ti-Ta-Sn metal foam SEM with 30% spacer (A). The EDS data suggest the presence of Ti, Ta and Sn alloying elements (B). Scanning electron microscopy (SEM) images, energy dispersive X-ray spectroscopy (EDS) spectra, and elemental mapping of Ti, Ta, and Sn (C).

The characterization by means of SEM shows the surface of the sample finding porosities and an alloy in a homogeneous way, there is an agglomeration of Ta powder that did not merge with the sample (Figure 1 A). Figure 1A also shows the differences in the chemical composition due to the contrast difference and the relief of the surface, the microporosity and macroporosity is caused by the sintering process, because the powder particles undergo deformation. Figure 1 B shows EDS quantitatively and qualitatively the mixture of Ti-Ta-Sn powders with a porosity of 30%. Figure 1C shows sample homogeneity, although, in some cases, it

presents a greater element of tantalum. In conclusion, the porosity obtained was good because it did not agglomerate spacer and left an excellent open porosity, the micropores and macropores should still be considered to have a better homogeneity and the pore shape is symmetrical. We can consider that this Ti-Ta-Sn metal foam alloy obtained by this method has great potential for biomedical applications.

References:

- Aguilar, C., Aguirre, T., Martínez, C., De Barbieri, F., San Martín, F., Salinas, V., Alfonso, I. (2020) Improving the mechanical strength of ternary beta titanium alloy (Ti-Ta-Sn) foams, using a bimodal microstructure, *Materials & Design* Volume 195, 108945, doi.org/10.1016/j.matdes.2020.108945.
- Geetha, M., Singh, A.K., Asokamani, R., Gogia, A.K. (2009). Ti-based biomaterials, the ultimate choice for orthopedic implants- a review. *Prog. Mater. Sci.*, 54, pp. 397-425, doi.org/10.1016/j.pmatsci.2008.06.
- Ryan, G., Pandit, A., Apatsidis, D.P. (2006) Fabrication methods of porous metals for use in orthopaedic applications. *Biomaterials* 27, 2651–2670 doi: 10.1016/j.biomaterials.2005.12.002
- Mejia, A., Béjar Gómez, L., Aguilar, C., Parra González, C., López, I.A. (2022) SEM Study of a Ti-Ta-Sn Ternary Alloy by Powder Metallurgy. *Microsc. Microanal.* 28 (Suppl 1). doi:10.1017/S1431927622010777.

SYNTHESIS OF SELENIUM NANONEEDLES FOR SOLAR CELLS AND PHOTOCELLS. ATIKURRAHMAN University of Arkansas at Little Rock, Department of Physics

Selenium, a critical element for photovoltaics and energy storage, is important in developing energy applications. Several methods have been used to synthesize selenium nanostructures, such as wet-chemistry, vapor growth, and pulsed laser ablation. This study introduces, for the first time, a new method of synthesizing selenium nanoneedles by pulsed laser ablation, different from e-beam lithography. The process involves 5 minutes of nanosecond Nd: YAG laser irradiation on a bulk selenium target in various organic solvents. The repetition rate of the laser pulse adjusts the aspect ratio, sharpness, and diameter of the nanoneedles. These nanoneedles have potential applications in optoelectronics for solar cells and photocells.

MICROSCOPIC ANALYSIS ON FIBERS, PLANT EXUDATES, INSECT PARTS AND PM_{2.5} AS POTENTIAL AEROALLERGENS CAUSING ALLERGIC REACTIONS. MARYTRINH NGUYEN, LYANNA DELEON, and NABARUN GHOSH

Department of Life, Earth and Environmental Sciences, West Texas A&M University, Canyon, Texas 79015

Due to the ever-increasing population growth and

industrial expansion, air quality in many cities continues to decline. In addition to naturally occurring aeroallergens such as pollen and fungi, particulate matter (PM) from wildfires, plant exudates, and insect parts contribute to increased particle pollution. Air samples have been obtained using a one-sided sticky tape wrapped around a drum inside a Burkard Volumetric Spore Trap. The Spore Trap was placed on the rooftop of ANB at West Texas A&M University. The collected samples on the exposed tape were stained and mounted on a slide for microscopic examination of aerosol debris including fibers, plant exudates, insect parts and PM_{2.5} through a BX-40 Olympus microscope for analysis. Plant exudates and insect parts in particular contain proteins that enter the respiratory system and trigger asthma symptoms. Fibers originating from cotton lint, feathers, and other stuffing materials may become airborne and carry other aeroallergens within them. In many of our slides, various forms of aeroallergens have been found on the slide to spread uniformly or in groups, or even attached to the fibrous material. Exudates from insects, plants, and even animals have an influence on indoor air quality and cause allergic symptoms especially due to chemicals in their urine and saliva. Therefore, there is an urgent need to develop an advanced air purification system to combat the severe effects of increased PM_{2.5} in the ambient air. In Mumbai, India, lung cancer deaths rose by nearly 49% between 2009 and 2021. Researchers cited the long exposure to air pollution, especially PM_{2.5}, and tobacco consumption as the reason behind the sharp increase. This is due to the highly vascularized alveoli and soft tissues of the lungs that easily absorb molecules from various substances, leading them to travel to different organs of the human body. Recently, the COVID-19 pandemic, as well as the severity of allergy cases, have been shown to be coupled with the increased number of wildfires across the United States. The frequency and intensity of wildfires is affected by climate change and produces smoke that has been shown to have delayed long-term effects in patients as long as one full year later. Clinical studies showed the number of doctor visits for asthma care increased during wildfires. Wildfires also have been shown to exacerbate susceptibility to SARS-CoV-2, positively associated with the number of daily cases, cumulative cases, and cumulative deaths. In our Aerobiology lab, we conducted a simulated experiment in a fiberglass chamber using the AFL Mini Air Sanifier and a Lighthouse Handheld Particle Counter to assess the indoor air quality by measuring the PM concentration of varying sizes. At different intervals, we recorded a decrease in concentration of PM_{2.5} when using the air purifier. We compared the PM counts when running and when not running the air purifier. The AFL Mini Air Sanifier has been shown to help reduce PM_{2.5} and improve indoor air quality by using AHPCO nanotechnology. Asthma patients are recommended to stay indoors, limit outdoor activities during high concentrations of PM_{2.5} and wear a mask for

outdoor activities. Therefore, close monitoring of the PM_{2.5} counts and preventive measures coupled with advanced air purification systems are crucial to combat unprecedented situations such as the COVID-19 pandemic and increasing allergy and asthma cases.

TECHNICAL ABSTRACTS Spring 2023

A NOVEL ION SOURCE FOR LITHIUM-ION MICROSCOPY AND 3D TOMOGRAPHY. JOSEPH KLINGFUS, KEVIN BURCHAM, and TORSTEN RICHTER

RAITH America, Inc. Troy, NY 12180

Liquid Metal Alloy Ion Source (LMAIS) is an emerging Focused Ion Beam (FIB) source technology. It has been established for nanofabrication over the last years (Gierak et al., 2018). Most recently, ion imaging with Lithium ions from GaBiLi eutectic alloy has become feasible (Klingner et al., 2020). Multiple ion species such as Lithium and Bismuth are emitted simultaneously from a single source and are separated in a subsequent Wien filter. Different ion species, light or heavy and fast or slow, can be selected quickly without any mechanical sample or column adjustment (Pilz et al., 2019).

Lithium is the lightest ion available from LMAIS. It features the smallest virtual source diameter and lowest energy spread (Bischoff et al., 2016). Hence, Lithium offers the smallest probe size of all ions emitted from eutectic alloys, resulting in sub 2 nm image resolution. Besides Lithium, Gallium and Bismuth ions, as well as Bi clusters, are available from the same source. Bismuth ions, and in particular Bi clusters, have an excellent depth of resolution for sample delayering. The combination of Bi and Li provides outstanding ion beam imaging capabilities.

Switching between Li and Bi can be accomplished within a few seconds and enables access to different ion beams within the same FIB column. This setup allows stable imaging of 3D structures and sample reconstruction. With the FIB system presented (here), Ion beams are always perpendicular to the sample and no stage movement or sample tilt is needed resulting in a stable and reliable process for tomography and 3D sample reconstruction.

In this contribution, we describe the working principle and capabilities of LMAIS with a focus on GaBiLi. Results of 2D Lithium-ion microscopy and workflows for stable 3D tomography by Bismuth milling and Li imaging will be presented.

References:

Gierak, J., Mazarov, P., Bruchhaus, L., Jede, R., Bischoff, L. (2018) Review of electrohydrodynamical ion

sources and their applications to focused ion beam technology. *Journal of Vacuum Science & Technology B* 36, 06J101.

Klingner, N., Hlawacek, G., Mazarov, P., Pilz, W., Meyer, F., Bischoff, L. (2020) Imaging and milling resolution of light ion beams from helium ion microscopy and FIBs driven by liquid metal alloy ion sources. *Beilstein J. Nanotechnology*, 11, 1742–1749.

Pilz, W., Klingner, N., Bischoff, L., Mazarov, P., Bauerdick, S. (2019) Lithium-ion beams from liquid metal alloy ion sources. *Journal of Vacuum Science & Technology B* 37, 021802.

Bischoff, L., Mazarov, P., Bruchhaus, L., Gierak, J. (2016) Liquid metal alloy ion sources—An alternative for focussed ion beam technology. *Appl. Phys. Rev.* 3, 021101.

UNIQUE ANALYTICAL COMBOs... THE ULTIMATE ANALYTICAL APPROACH. JOHN MASTOVICH Bruker AXS Inc., Madison, WI 53711

The Scanning Electron Microscope (SEM) using electron beam excitation and Energy-Dispersive (EDS) detector has become the industry standard, as throughput and general performance have steadily improved. Today, MicroXRF technologies are available, providing very high X-ray flux with Trace Analysis and rapid data acquisition. The unique Dual Excitation approach provides many analytical advantages beyond trace detection, when dealing with beam sensitive low voltage applications and yields the ultimate Trace Analysis throughput and workflow.

Numerous applications ranging from soft materials (polymers & biologicals) to devices (microelectronics & semiconductor) and materials (metals & composites) will be discussed to illustrate the analytical benefits of the Dual Excitation approach. A significant advantage is the enabling of low dose/low voltage applications, while also using X-ray excitation to observe the extended range of the spectrometer as depicted in Figure 1A and 1B. Clear data are generated from samples that typically produce few to no X-rays via e-beam, from depths of many microns from within the sample, as shown in Figure 1C. When the ultimate spectral and spatial resolution is required, the data in Figure 1D conveys Wavelength Dispersive Spectroscopy (WDS).

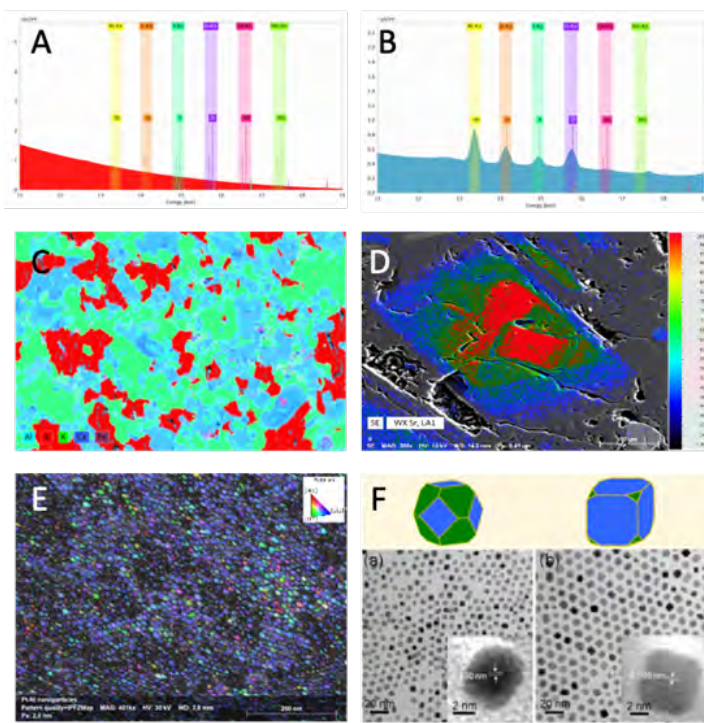


Figure 1. SOLEIL synchrotron facility. Used with permission (https://commons.wikimedia.org/wiki/File:SOLEIL_le_01_juin_2005.jpg)

Figure 1. Analytical benefits of Dual Excitation approach in SEM. a) Electron beam excitation; b) X-ray beam excitation; c) MicroXRF elemental mapping; d) Wavelength dispersive mapping; e) Platinum Nickel nanocrystals; f) Bright and dark field like imaging.

Simultaneous EDS - Electron Backscatter Diffraction (EBSD) is possible from thinned samples, gathering the utmost spatial resolution during *in-situ* work as illustrated in Figure 1E and 1F.

Overall, due to the FlatQUAD detector to the sample design, the *in-situ* work provides superior collection efficiency regardless of whether the SEM or Scanning Transmission Electron Microscopy (STEM) applications are implemented.

RECENT ADVANCES IN THE USE OF LABORATORY MICROXRF AS A SCREENING TOOL FOR MICROSYNCHROTRON RADIATION X-RAY FLUORESCENCE SPECTROMETRY. ROBERT C. TISDALE
IXRF, Inc., Austin, TX, USA.

Synchrotron facilities (like that shown in Figure 1) provide electromagnetic radiation ranging from infrared to X-ray with high brightness, high collimation and wide tunability. These properties make synchrotron radiation an ideal light source for a number of spectroscopic applications. Among different synchrotron-based techniques, X-ray absorption spectroscopy (XAS), X-ray emission spectroscopy (XES), X-ray photoelectron spectroscopy (XPS) and X-ray fluorescence spectroscopy (XRF & microXRF) are widely used (Wu et al. 2014).

The first analytical microprobe using synchrotron radiation excitation (microXRF) was demonstrated at the Cambridge Electron Accelerator by Paul Horowitz and John Howell. They focused the X-ray beam with a bent cylindrical mirror and defined a beam spot with a pinhole in front of the target. The pinhole was as small as 2 μm (Jones et al 1985). In their first report, published in Science (August 1972), the authors described the XY-scanning prototype design and presented results obtained during initial weeks of operation. It was their hope that some of the unique characteristics of this first X-ray Microscope (XRM) might be ultimately useful to a variety of disciplines (Horowitz et al. 1972).

Subsequent review papers by Bernasconi and Adams, 1994; Adams et al., 1998, Rivers et al., 2008; Fittschen and Falkenberg, 2011; Gardea-Torresdey, 2012; Pushie et al., 2014; Wang et al., 2018; Feng et al., 2020; and Warlo et al., 2022 serve to illustrate later advances in both laboratory and synchrotron microXRF technologies and techniques. While synchrotrons have gotten ever more powerful, with modern optics delivering very intense micro X-ray spots, there are nevertheless limitations with which to contend. Key factors in making these facilities attractive and productive for users include familiarity of operational procedures and the availability of experimental techniques and features normally found in their home laboratories. A variety of additional factors may also contribute to limited beamline access, including beamline or ring downtime, shared physical resources that require reconfiguration for microXRF experiments, lack of beamline staff, excessive demand for beam time (like experienced with the FedEx crystallography boom), as well as travel and beam reservation disruptions ... to name but a few.

Typically, beamtime at synchrotron facilities is limited, stifling experimental immediacy that is critical to the smooth flow of experimental design. In 2013, Pemmer, et al. set out to create a homemade laboratory based microXRF system to examine the efficacy of

such a tool for enhancing microsynchrotron radiation X-ray fluorescence (microSRXRF) utilization efficiency. Their team's system consisted of a low power Mo-anode X-ray tube (50W) coupled to a polycapillary optic and 30 mm² Si (Li) detector. Housed in a vacuum chamber, this X-ray spectrometer – with a 50 μm spot size at the sample position – was tested to see if this setup could be used as pre-screening tool for the XAS beamline at the ANKA radiation facility within the Karlsruhe Institute of Technology (Karlsruhe, Germany). Results from a rat animal model obtained with microSRXRF were compared to measurements of the same samples in the laboratory. Despite the inferior measurement conditions in the laboratory compared to the synchrotron, the same significant differences were found for the different treatment groups in the study. Their conclusion was that the idea of using a laboratory microXRF system, as an easily accessible screening tool for synchrotron studies, was indeed reasonable (Pemmer, 2013) It is worth noting that, as detailed in the scientific literature, other homemade microXRF systems have been developed at synchrotron facilities due to similar drivers that motivated Pemmer (Adams et al., 1998).

Thirty-one years ago, Kevex Instruments (dissolved) introduced the world's first fully automated, general purpose, high resolution microXRF imaging spectrometer. With a 50 μm minimum spot size, coupled to a computer controlled XYZ-stage, the Kevex Omicron was revolutionary in concept and function. With a tube-below design, it was as capable with bulk samples (liquids and powders) as it was with semiconductor wafers. The only real drawback was that, since polycapillary optics were not yet commercially available, mapping times could be glacial with the 50 μm pinhole spot (Tisdale, 2022).

X-ray optics have long been the domain of the synchrotron world, but most of the advances were not readily applicable to the commercial energy dispersive X-ray fluorescence (EDXRF) industry. All that changed with the commercialization of Kumakhov (polycapillary) optics in the late 1990s. Compact low wattage microfocus X-ray tubes were suited to be mated with such optics to afford “white” X-ray sources with micron scale spatial resolution (at the focal point) and exceptional fluence.

Since 2014, commercial laboratory microXRF systems, suitable for beamline screening, have taken the form of both benchtop systems, with a somewhat constricted vacuum chamber size, or large freestanding spectrometers. Some of the largest systems do not offer vacuum atmosphere analyses, and therefore are not suitable for low-Z applications. In cases where bench space and/or floorspace is limited, there is yet another option: microXRF within a scanning electron microscope (SEM-XRF). A microXRF X-ray source may be added to almost any “column type” SEM with an available high-angle port.

Two recent papers by van der Ent (2021) and

Ren (2022) compared microXRF results obtained at the synchrotron with those acquired with modern commercial laboratory instrumentation (see Figures 2 and 3). The latter paper compared data on leaves from *Gossia fragrantissima*. While the spatial resolution of laboratory data was an order of magnitude larger in this case, it should be noted that laboratory microXRF systems are available with focused beams down to 5μm diameter spot size. Of course, data collection times are much quicker at the synchrotron.

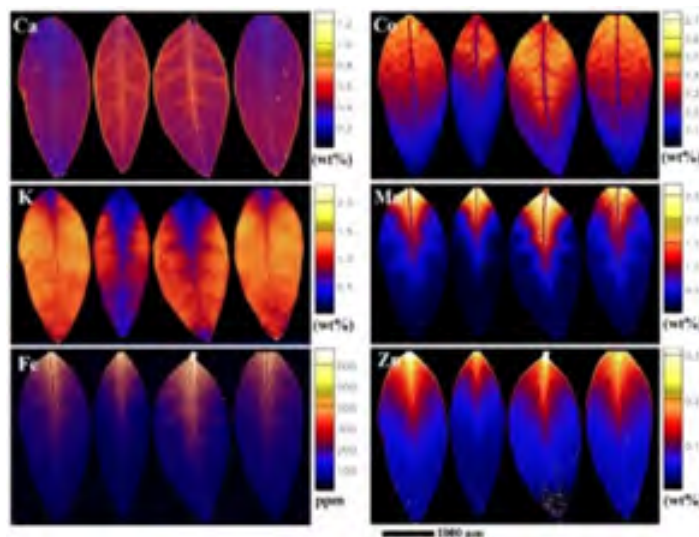


Figure 2. Synchrotron microXRF at 2μm resolution. From van der Ent A. et al., 2021; Images used with permission.

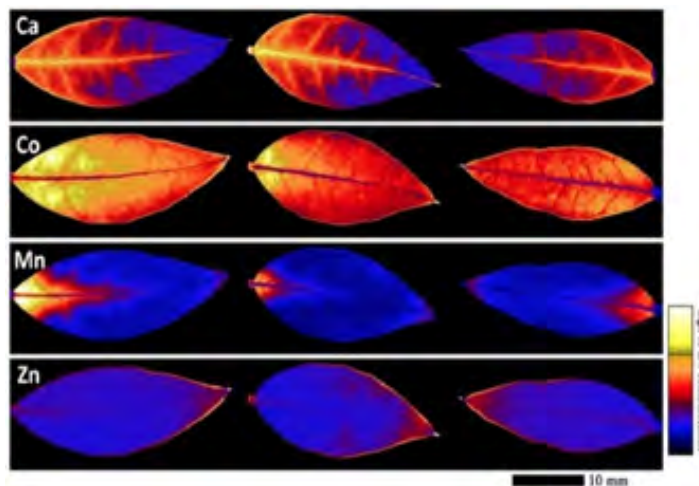


Figure 3. Laboratory microXRF at 25μm resolution. From van der Ent A. et al., 2021; Images used with permission.

References:

- Wu, P., Yu, Y., McGhee, C. E., Tan, L. H., & Lu, Y. (2014). Applications of synchrotron-based spectroscopic techniques in studying nucleic acids and nucleic acid-functionalized nanomaterials. *Advanced Materials*, 26(46), 7849-7872.
- Jones, K.W. et al. (1985) Design criteria and sensitivity calculations for multielemental trace analysis at the NSLS X-ray microprobe. *Nuclear Instruments and Methods B*, V. 10-11, Pt. 1, 293-298.
- Horowitz, P. and Howell, J.A. (1972) A Scanning X-Ray Microscope Using Synchrotron Radiation. *Science*, 178 (4061). DOI: 10.1126/science.178.4061.608.
- Bernasconi, G. and Adams, et al. (1994). Microscopic X-ray Fluorescence Analysis. *J. Anal. Atomic Spectrometry*, Vol. 9, 151-157.
- Pushie, M.J. et al. (2014) Elemental and Chemically Specific X-ray Fluorescence Imaging of Biological Systems. *Chemical Reviews*, 114, 8499-8541.
- Fittschen, U.E.A. and Falkenberg, G. (2011) Trends in environmental science using microscopic X-ray fluorescence. *Spectrochimica Acta Part B: Atomic Spectroscopy*, Volume 66, Issue 8, 567-580.
- Gardea-Torresdey, J.L. (2012) Applications of synchrotron μ -XRF to study the distribution of biologically important elements in different environmental matrices: A review. *Analytica Chimica Acta*, Vol. 755, 1-16.
- Adams, F., et al. (1998) Microscopic X-ray fluorescence analysis and related methods with laboratory and synchrotron radiation sources. *J. Anal. Atomic Spect.*, Vol. 13, 319-331.
- Rivers, M.L., et al. (2008) Synchrotron X-ray fluorescence microscopy. *Synch. Rad. News*, Vol. 4, No 2. 23-26.
- Wang, P., et al. (2018) Synchrotron-Based X-Ray Fluorescence Microscopy as a Technique for Imaging of Elements in Plants. *Plant Physiol.* 178(2): 507-523.
- Warlo, M., et al. (2022) Extreme-resolution synchrotron X-Ray fluorescence mapping of ore samples. *Ore Geology Reviews* 140, 104620.
- Feng, X., et al. (2020) X-ray fluorescence application in food, feed, and agricultural science: a critical review. *Critical Rev. in Food Science and Nutrition*. Vol 61, No. 14, 2340-2350.
- Pemmer, B. (2013). Synchrotron micro-X-ray fluorescence imaging of trace elements in articular cartilage and bone in health and disease. *repositUM*. Technischen Universität Wien.
- Adams, F., et al. (1998) Microscopic X-ray fluorescence analysis and related methods with laboratory and synchrotron radiation sources. *J. Anal. Atomic Spect.*, Vol. 13, 319-331.
- Tisdale, R. (2022) Recent Advancements in Integrated X-ray Sources for Scanning Electron Microscopy [Conference presentation]. Texas Society for Microscopy @ Baylor U., Waco, TX, USA.
- van der Ent, A. et al. (2021) Incidence of hyperaccumulation and tissue-level distribution of manganese, cobalt, and zinc in the genus *Gossia* (*Myrtaceae*). *Metallomics*. Apr 4;13(4):mfab008 (images used with permission)
- ZW Ren, et al. Fast X-ray fluorescence microscopy provides high-throughput phenotyping of element distribution in seeds. *Plant Physiol.* 2022 Nov 24:kiac534.

CALL FOR PAPERS

Authors are invited to submit their manuscripts for the next edition of the Texas Journal of Microscopy. The objective of the journal is to publish papers on original research and developing methods for providing prospect guidelines to research supported by all forms of microscopy. Please send your work as short communications, full articles or review articles in biological sciences, material sciences and/or education to the journal editor.

Catalina Iulia Pislariu, PhD
cpislariu@twu.edu

VISIT THE TSM WEBSITE

<https://texas.microscopy.org/>



Advancing Microscopy and Microanalysis



Embracing All Forms of Microscopy

[HOME](#) [ABOUT](#) [MEMBERSHIP](#) [EVENTS](#) [SMALL GRANT](#) [JOURNAL](#) [CONTACT US](#)  

Welcome to the Texas Society for Microscopy

About Us

The Texas Society for Microscopy (TSM) was founded in 1963 and has become an informative resource for many scientists since then. We welcome microscopists, researchers, students and administrators from all disciplines and backgrounds who are interested in microscopy or the science of microscopy.

Our non-profit organization is committed to advancing knowledge and understanding of all aspects of microscopy and their applications as they apply to life sciences, materials sciences and industry. We are committed to support students through our **Small Grant Program** and through travel grants to attend our annual meetings. The society is also represented at the meetings of the Microscopy Society of America through our president. The annual meetings of the TSM are a highlight for our members and enjoy wide corporate support.

We invite you to become a member of the TSM and support its mission and vision through your membership.

AN AFFILIATE OF THE



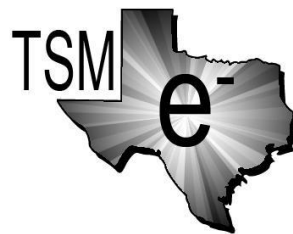
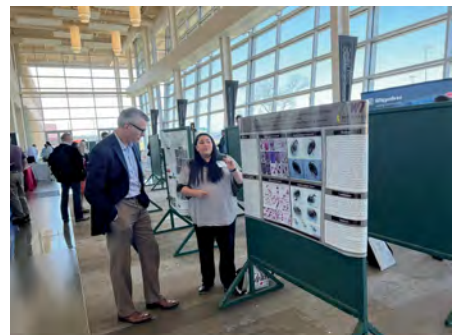
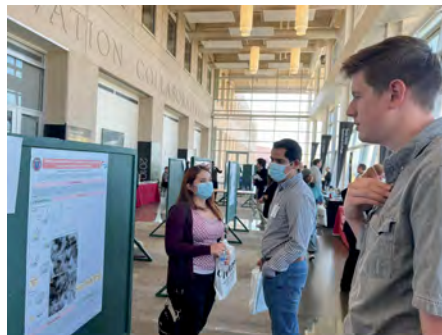
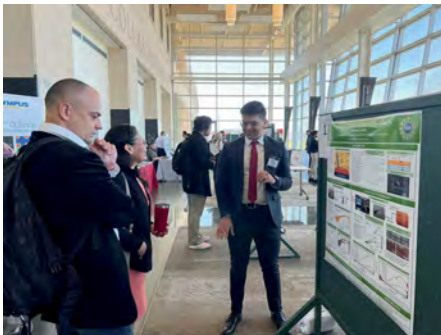
AN AFFILIATE OF THE



The 56th Texas Society for Microscopy Meeting

March 24-25, 2022

Baylor Research and Innovation Collaborative (BRIC), Waco, TX



Advancing Microscopy and Microanalysis

Corporate Members and Regional Sales Managers



Andor Instruments, an Oxford Company

<https://andor.oxinst.com/>
860 Aviation Pkwy Ste 1400
Morrisville, NC 27560
Phone: 408-850-1139
Bruno Combettes
Phone: 978-402-5023; b.combettes@andor.com
Ryan Robinson
Phone: 978-402-5023; r.robinson@andor.com
Tomas Silvia Santisteban
Phone: 978-402-5023; t.silva@bitplane.com



Advanced Microscopy Techniques

Advanced Microscopy Techniques
<http://www.amtimaging.com>
242 West Cummings Park
Woburn, MA 01801
Tom Levesque
Phone: 214-883-3194; tlevesque@amtimaging.com



AMETEK, GATAN, EDAX

<http://www.ametek.com>
85 Mckee Dr.
Mahwah, NJ 07430-2105
Phone: 201-466-0907
John Haritos
Phone: 201-466-0907; John.haritos@ametek.com
David Stowe; David.Stowe@ametek.com



AVR Optics

www.avr-optics.com
187 N Water Street
Rochester, NY 14604
Lane Manning
Phone: 585-445-7588; lane.manning@avr-optics.com



Agilent Technologies

BioTek Instruments, Inc. (Now Agilent)

<http://www.biotek.com>
5301 Stevens Creek Blvd.
Santa Clara, CA 95051
David Kurtz
Phone: 847-757-3387; kurtzd@biotek.com
Richard Westhoven
Phone: 512-2025588; richard.westhoven@agilent.com



Boeckeler Instruments, Inc.

<http://www.boeckeler.com>
4650 S. Butterfield Drive
Tucson, AZ 85714
Phone: 520-745-0001
Fax: 520-745-0004
Peter Strucks
Phone: 520-331-2216
peter.strucks@boeckeler.com



Bruker AXS, Inc.

www.bruker.com
3194 Beverly Court
Murrysville, PA 15668
Phone: 908-419-8225
Austin, TX 78747
John Mastovich
Phone: 908-419-8225; john.mastovich@bruker.com



CARL ZEISS MICROSCOPY

<http://www.zeiss.com/nts>
Laura Grafflin
One corporation Way
Peabody, MA 01960
Phone: 978-826-1500
Fax: 978-532-5696 Fax
Laura Grafflin
Phone: 214-924-7249; laura.grafflin@zeiss.com
Philipp Bastians
Phone: 914-7471800; philipp.bastians@zeiss.com
John Donlon
Phone: 800-233-2343; john.donlon@zeiss.com



Discover Echo Inc.

<https://discover-echo.com/>
9530 Padgett St., Suite 101
San Diego, CA 92126
Adam Conway
Phone: 617-999-2774;
aconway@discover-echo.com
Joanna Harper
Phone: 617-999-2774;
jharper@discover-echo.com
Brian Templin
Phone: 713-557-8915;
btemplin@discover-echo.com



Electron Microscopy Science/Diatome

<http://www.emsdiasum.com/microscopy/>
1560 Industry Road, P.O. BOX 550
Hatfield, PA 19440
Phone: 800-523-5874
Fax: 215-412-8450
Stacie Kirsch
Phone: 215-415-8400;
Stacie@ems-secure.com
Robert Armstrong
Phone: 215-412-8400;
rarmstrong@emsdiasum.com



E.A. Fischione Instruments, Inc.

<http://www.fischione.com>
9003 Corporate Circle
Export, PA 15632
Phone: 724-325-5444
Nicole Dengler
Phone: 724-325-5444; nm_dengler@fischione.com



Hitachi High Technologies America

<http://www.hitachi-hita.com>
1375 North 28th Ave.
PO Box 612208
Irving TX 75261
Phone: 214-537-2158
Fax: 972-615-9300
Robert Passeri
Phone: 847-946-3788; robert.passeri@hitachi-hightech.com
Matthew Reinoehl
Phone: 847-946-3788; matthew.reinoehl@hitachi-hightech.com



IXRF Systems

<http://www.ixrfsystems.com>
10421 Old Manchaca Rd., Suite 620
Austin, TX 78748
Phone: 512-386-6100
Fax: 512-386-6105
Bryan De Verse
Phone: 512-386-6100; bryand@ixrfsystems.com
Mandi Chukwu
Phone: 512-386-6100; mandih@ixrfsystems.com
Andrea Surak; andreas@ixrfsystems.com
Robert Tisdale
Phone: 512-415-6839; robertt@ixrfsystems.com



Solutions for Innovation

JEOL USA, Inc.

<http://www.jeolusa.com>
13810 Paisano Circle
Austin, TX 78737
Phone: 978-495-2176
Joel Paul
Phone: 978-979-8071; jpaul@jeol.com



MICROSYSTEMS

Leica Microsystems, Inc.

<http://www.leica-microsystems.com>
7125 Northland Terrace N., Suite 100
Brooklyn Park, MN 55428
Phone: 314-374-9361
Andrew Lawson
Phone: 469-785-9992
Andrew.Lawson@leica-microsystems.com
Nancy Rizzo
Phone: 224-532-6297
Nancy.Rizzo@leica-microsystems.com



Marine Reef International

<https://www.marinereef.com/>
1048 Irvine Avenue
Suite 634
Newport Beach, CA 92660
Phone: 949-723-0283
Linda Dailey
Phone: 903-851-5187; lindasdailey@gmail.com



M.E. Taylor Engineering, Inc.

<http://www.semsupplies.com>
SEMico Division
15817 Crabbs Branch Way
Rockville, MD 20855
Gene Taylor
Phone: 301-975-9798; sales@semicro.org



Molecular Devices, LLC.

<https://www.moleculardevices.com/>
3860 North First Street
San Jose, CA 95134
Phone: 800-635-5577
Robert Moody
Phone: 469-662-8381; robert.moody@moldev.com
Mridula Vishwanath
Phone: 469-662-8381
mridula.vishwanath@moldev.com



a Thomas Scientific, LLC company

NCI, Inc.

<https://www.ncimicro.com/>
7125 Northland Terrace N, Suite 100
Brooklyn Park, MN 55428
Phone: 888-559-3312
Mike Hehr
Phone: 314-374-9361; mikeh@ncimicro.com
Michael May
Phone: 405-788-0775; michaelm@ncimicro.com



Nikon Instruments Inc.

<http://www.nikoninstruments.com>
1300 Walt Whitman Road
Melville, NY 11747-3064
Phone: 972-693-7779
Jonathan Ekman
Phone: 407-595-6542;
jonathan.ekman@nikon.com
Kara Harmatys
Phone: 713-301-9932;
kara.harmatys@nikon.com



Olympus America Inc.

www.olympus-lifescience.com
48 Woerd Ave.
Waltham, MA 02453
Phone: 512-230-5624
Brian Cook
Phone: 512-230-5624;
Brian.Cook@olympus-ossa.com
Ashley Divine
Phone: 832-243-7982;
ashley.divine@olympus.com
Lance Hall
Phone: 512-230-5624;
Lance.hall@olympus-ossa.com
Doug Kennedy
Phone: 512-230-5634;
doug.kennedy@olympus-ossa.com
Joseph Lake
Phone: 469-580-7565;
joseph.lake@olympus.com



Oxford Instruments America, Inc.

www.oxford-instruments.com
300 Baker Avenue, Suite 150
Concord, MA 01742
Phone: 978-369-9933 x 201
Sonika Robertson
Phone: 987-402-5983;
sonika.robertson@oxinst.com



Protochips

www.protochips.com
3800 Gateway Centre Blvd., Suite 306
Morrisville, NC 27560
Phone: 919-377-0898
Mike Coy
Phone: 612-751-4391; mike.coy@protochips.com
Dylan Wood
Phone: 612-751-4391;
Dylan.Wood@protochips.com



RAITH America

https://raith.com/
300 Jordan Road
Troy, NY 12180
Phone: 518-874-3000
Kevin Burcham
Phone: 701-238-1267;
kevin.burcham@raithamerica.com
Joseph Klingfus
Phone: 701-238-1267;
Joseph.klingfus@raithamerica.com



TESCAN USA, Inc

http://www.tescan-usa.com
765 Commonwealth Drive, Suite 101
Warrendale, PA 15086
Phone: 512-417-8990
Mike Craig
Phone: 724-772-7433; mike.craig@tescan-usa.com



Leading With Innovation

Rigaku

www.rigaku.com
9009 New Trails Dr.
The Woodlands, TX 77381
Phone: 281-362-2300 ext. 122
Angela Criswell
Phone: 281-362-2300; angela.criswell@rigaku.com
Michelle Goodwin
Phone: 281-362-2300;
Michelle.Goodwin@rigaku.com
Michael Holcomb
Phone: 281-362-2300;
Michael.Holcomb@rigaku.com
Aya Takase
Phone: 281-362-2300; Aya.Takase@rigaku.com



Microscopy Products for Science and Industry

Ted Pella, Inc.

http://www.tedpella.com
PO Box 462477
Redding, CA 96049-2477
Phone: 530-243-2200 or 800-237-3526
James Long
Phone: 530-227-8329; James_Long@tedpella.com
David Rollings
Phone: 530-243-2200; sales@tedpella.com
Kathy Stangenberg
Phone: 530-243-2200; sales@tedpella.com



Texas A&M University, School of Medicine

Integrated Microscopy Imaging Laboratory
https://medicine.tamu.edu/imil/index.html
8447 Riverside Pkwy
Bryan, TX 77807
Malea Murphy
Phone: 979-436-9037; maleamurphy@tamu.edu



The rising STAR of Texas

Texas State University

Shared Research Operations
https://sro.txstate.edu/
601 University Drive
San Marcos, TX 78666
Phone: 512-245-6635
Alissa Savage
Phone: 512-213-7909; as59@txstate.edu
Casey Smith
Phone: 512-213-7909; cs53360@txstate.edu



FEI / Thermo Fisher Scientific

https://www.thermofisher.com
http://www.fei.com
K.D. Derr
Phone: 619-944-7633;
kd.derr@thermofisher.com
Bill Sgammato
Phone: 508-479-6623;
bill.sgammato@thermofisher.com
Dan Snyder
Phone: 346-423-8193;
dan.snyder@thermofisher.com
Ciceron Yanez
Phone: 281-739-7370;
ciceron.yanez@thermofisher.com



Tousimis

http://www.tousimis.com
2211 Lewis Avenue
Rockville, MD 20851
Phone: 301-881-2450
Fax: 301-881-5374
Hyun Park
Phone: 301-881-2450; hjpark@tousimis.com





Eastern redbud (*Cercis canadensis*, Fam. *Fabaceae*), a Texas native tree, in bloom. Flowers develop in spring before leaves emerge (A, B). Scanning Electron Microscopy (SEM) micrograph of pollen grains (C). Scale bar: 20 μm . Photos courtesy of Dr. Camelia Maier, Texas Woman's University

ELECTRON MICROSCOPY SCIENCES...

your source for the latest,
the best, the most advanced

NEW PRODUCTS



Please visit our website to view or download our **NEW PRODUCT FOCUS** Catalog, featuring all these products and dozens more.

Diamond[®] SureFlow[™] Bottle Top Dispensers

Precise and easy dispensing of laboratory reagents with an ergonomic design.



DYMO-Compatible Cryogenic Labels

Including CryoSTUCK[®] Thermal Transfer Labels and Freezer-DTermo[™] Deep Freeze Labels.



Fast-Cooling Non-Stick Metal Base Molds

Reuseable and disposable molds also available.



ClariTex Slides

Ready-to-use slides are manufactured from super grade glass with uniform thickness, fulfilling optical requirements for light microscopy.

CellCeps+ Heated Forceps

For orientation and positioning of histological specimens during embedding in paraffin wax.



Vortex[™] Biopsy Cassettes

Small and Micro size. Biopsy Paper as well!



PEN Foil Bottom Sterile Dishes

Ideal for laser microdissection.



Electron Microscopy Sciences

P.O. Box 550 • 1560 Industry Rd. • Hatfield, PA 19440
Tel: (215) 412-8400 • Fax: (215) 412-8450
email: info@emsdiasum.com or stacie@ems-secure.com

www.emsdiasum.com

EMS has it!

Scan here to view our **NEW PRODUCT FOCUS** as a downloadable PDF...





Salamander, Epidemio, Cilia - Louise Lewis
Bioscience Electron Microscopy Lab, University of Conn

Facial Nanotruss
Caltech, Materials Science and Mechanics (Julia R. Greer & Greg Group)

Multi-Application Autosamdri®-931 CPD System

- ✓ *NEW ! Post Process Data Review Feature*
- ✓ *Default "Automode" Setting Suitable for Most Applications*
- ✓ *Patent Pending "Stasis Software" for Challenging Sample Types*
- ✓ *Automatic & Custom Programmable Recipe Capability*
- ✓ *Available in Three Chamber Sizes*
- ✓ *Cleanroom System Options*
- ✓ *Made in U.S.A.*